AD-A092 711 BOLT BERANEK AND NEWMAN INC ARLINGTON VA F/G 9/5
EFFECTS OF INPUT POWER FLUCTUATION ON PASSIVE SONAR RECEIVER PE--ETC(U)
SEP 80 M MOLL, D D GOODMAN N00014-79-C-0446
UNCLASSIFIED BBN-4262 NL

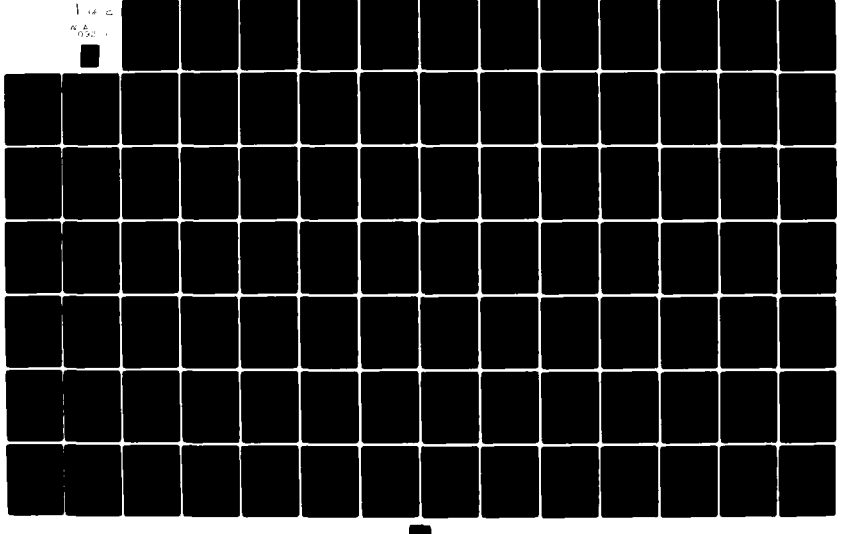

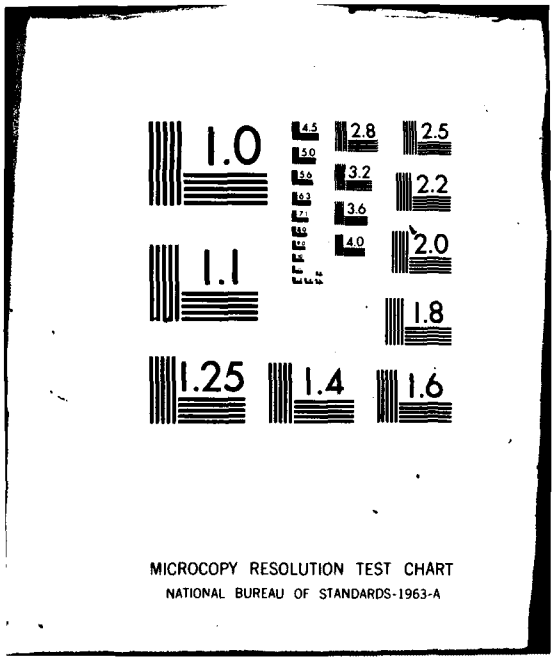
1.0
1.1
1.25
1.4
1.6
1.8
2.0
2.2
2.5
2.8
3.2
3.6
4.0
4.5
5.0
5.6
6.3
MICROCOPY RESOLUTION TEST CHART
NATIONAL BUREAU OF STANDARDS-1963-A

(12)

BBN Report No. 4262

EFFECTS OF INPUT POWER FLUCTUATION ON PASSIVE SONAR RECEIVER PERFORMANCE

M. Moll
D. Goodman

September 1980

Prepared for:

Naval Analysis Program
N00014-79-C-0446 NR 274-313

Prepared by:

Bolt Beranek and Newman Inc.
1701 North Fort Myer Drive
Arlington, VA 22209

BBN Report No. 4262

EFFECTS OF INPUT POWER FLUCTUATION ON PASSIVE SONAR RECEIVER PERFORMANCE

M. Moll
D. Goodman

September 1980

Prepared for:

Naval Analysis Program
N00014-79-C-0446 NR 274-313

Prepared by:

Bolt Beranek and Newman Inc.
1701 North Fort Myer Drive
Arlington, VA 22209

(12) 112

UNCLASSIFIED

(17) BBN-4262

SECURITY CLASSIFICATION OF THIS PAGE (When Data Entered)

REPORT DOCUMENTATION PAGE

READ INSTRUCTIONS BEFORE COMPLETING FORM

1. REPORT NUMBER: BBN Report No. 4262
2. GOVT ACCESSION NO.: AD-A092711
3. RECIPIENT'S CATALOG NUMBER:

4. TITLE (and Subtitle): (6) Effects of Input Power Fluctuation on Passive Sonar Receiver Performance.
5. TYPE OF REPORT & PERIOD COVERED: (9) Technical rept.,
6. PERFORMING ORG. REPORT NUMBER: BBN Report No. 4262

7. AUTHOR(S): (10) M. Moll, D.D. Goodman
8. CONTRACT OR GRANT NUMBER(S): (15) N0014-79-C-0446

9. PERFORMING ORGANIZATION NAME AND ADDRESS: Bolt Beranek and Newman Inc., 1701 North Fort Myer Drive, Arlington, VA 22209
10. PROGRAM ELEMENT, PROJECT, TASK AREA & WORK UNIT NUMBERS: 65152N RO145-TW NR 274-313

11. CONTROLLING OFFICE NAME AND ADDRESS: Naval Analysis Program (Code 431), Office of Naval Research, Arlington, VA 22217
12. REPORT DATE: Sep[illegible] 1980
13. NUMBER OF PAGES: 106

14. MONITORING AGENCY NAME & ADDRESS (if different from Controlling Office): N/A (16) RO145TW
15. SECURITY CLASS. (of this report): UNCLASSIFIED
15a. DECLASSIFICATION/DOWNGRADING SCHEDULE: N/A

16. DISTRIBUTION STATEMENT (of this Report)

"Approved for Public Release; Distribution Unlimited"

17. DISTRIBUTION STATEMENT (of the abstract entered in Block 20, if different from Report)

N/A

18. SUPPLEMENTARY NOTES

19. KEY WORDS (Continue on reverse side if necessary and identify by block number)

Passive Sonar Detection Performance
Underwater Acoustic Fluctuations

20. ABSTRACT (Continue on reverse side if necessary and identify by block number)

Abstract. Passive sonar receivers operate in environment producing signals and noise with fluctuating power envelopes. The effect of these fluctuations on receiver performance was investigated by means of a Monte Carlo simulation in which signals and noise were represented by members of compound random processes. The receiver was represented by a multichannel analog with an adaptive detection threshold. It was determined that both detection and false alarm probability depend on the

DD FORM 1 JAN 73 1473 EDITION OF 1 NOV 65 IS OBSOLETE

UNCLASSIFIED

SECURITY CLASSIFICATION OF THIS PAGE (When Data Entered)

406454

20. relationship of the relaxation times of the input power envelopes and the post-rectification averaging time of the receiver, as well as on the degree of fluctuation.

TABLE OF CONTENTS

1.0 INTRODUCTION AND SUMMARY..... 1-1

2.0 SIMULATION..... 2-1

2.1 Sampled Data Multichannel Analog and Inputs..... 2-1
2.2 Estimation of Probabilities..... 2-7

3.0 SPECIAL CASE: GAUSSIAN NOISE INPUTS..... 3-1

3.1 Introduction..... 3-1
3.2 Skewness and Kurtosis..... 3-3
3.3 Probability Density..... 3-5
3.4 False Alarm Probability..... 3-11

4.0 NOISE AND SIGNAL CHARACTERIZATION..... 4-1

4.1 Introduction..... 4-1
4.2 Envelope Estimation..... 4-7

5.0 FALSE ALARM PROBABILITY - COMMON NOISE POWER ENVELOPE..... 5-1

6.0 DETECTION PROBABILITY - COMMON NOISE POWER ENVELOPE..... 6-1

6.1 Gaussian Signals and Noise..... 6-1
6.2 Limiting Case - Very Fast Fluctuations..... 6-5
6.3 Limiting Case - Very Slow Fluctuations..... 6-8
6.4 Transition Curves..... 6-9

7.0 PARTIALLY-CORRELATED NOISE POWER ENVELOPES..... 7-1

7.1 Introduction..... 7-1
7.2 Limiting Case - Very Slow Fluctuations..... 7-4
7.3 Limiting Case - Very Fast Fluctuations..... 7-5

TABLE OF CONTENTS (CONTINUED)

7.4 False Alarm Probability..... 7-9
7.5 Transition Curves..... 7-11

REFERENCES..... R-1

APPENDIX A..... A-1

APPENDIX B..... B-1

LIST OF FIGURES

FIGURE 2.1	Channel with Threshold Formation	2-2
FIGURE 2.2	Equivalent Operations	2-2
FIGURE 2.3	Input Generation	2-4
FIGURE 2.4	Power Envelope Formation	2-4
FIGURE 2.5	Square of Noise Input	2-6
FIGURE 2.6	Simplified Operation	2-6
FIGURE 2.7	Common Noise Power Envelope	2-8
FIGURE 2.8	Equivalent Threshold	2-8
FIGURE 3.1	Density of Output for $n = 60$	3-9
FIGURE 3.2	Density of Output for $n = 14$	3-9
FIGURE 3.3	Density of Output for $n = 30$	3-10
FIGURE 3.4	Density of Output for $n = 60$	3-10
FIGURE 3.5	P_F and P_A for $n = 6$	3-13
FIGURE 3.6	P_F and P_A for $n = 14$	3-13
FIGURE 3.7	P_F and P_A for $n = 30$	3-14
FIGURE 3.8	P_F and P_A for $n = 60$	3-14
FIGURE 4.1a	Low-Band Envelope Spectrum - Nearly Horizontal Elevation	4-9
FIGURE 4.1b	High-Band Spectrum of a Nearly Horizontal Elevation	4-9
FIGURE 4.2a	Low-Band Envelope Spectrum - Overhead Elevation	4-11
FIGURE 4.2b	High-Band Envelope Spectrum of the Overhead Elevation	4-11
FIGURE 4.3a	Low-Band Envelope Spectrum - Single Element	4-12
FIGURE 4.3b	High-Band Envelope Spectrum of a Single Element	4-12
FIGURE 4.4	Intensity correlation for the upper (top figure) and lower (bottom figure) paths at 2250 Hz	4-16
FIGURE 4.5	Normalized autocovariance function for amplitude fluctuations	4-16

LIST OF FIGURES (CONTINUED)

FIGURE 5.1	Simulation Analog for False Alarm.....	5-7
FIGURE 6.1	Detection Simulation - Common Noise Power Envelope.....	6-2
FIGURE 6.1	Noise Power Envelope Detection Simulation - Common.....	6-2
FIGURE 6.2	Transition Curve for n = 60.....	6-4
FIGURE 6.3	Transition Curves.....	6-10
FIGURE 6.4	Transition Curves - Common Noise Power Envelope.....	6-11
FIGURE 7.1	Synthesis of Partially-Correlated Noise Power Envelope..	7-2
FIGURE 7.2	Detection Simulation-Partially-Correlated Noise Power Envelope.....	7-3
FIGURE 7.3	Effect of Correlation of Noise Power Envelope - Very Slow Fluctuations.....	7-6

LIST OF TABLES

TABLE 2.1	Confidence limits for p	2-10
TABLE 3.1	Salient Features of f(c)	3-4
TABLE 3.2	Salient Features of g(c)	3-5
TABLE 3.3	Measures and Moments	3-8
TABLE 5.1	False Alarm Probability - Fast Fluctuations	5-5
TABLE 5.2	False Alarm Probabilities - Various Cases	5-8
TABLE 6.1	Comparison of Simulation and Calculation	6-5
TABLE 6.2	Threshold and Spread Values - Common Noise Power Envelope	6-12
TABLE 7.1	False Alarm Probability - Partially Correlated Envelope.	7-10
TABLE 7.2	Threshold and Spread Values-Partially-Correlated Noise Power Envelopes	7-12
TABLE A-1	False Alarm Probability	A-4
TABLE A-2	False Alarm Probability - P_F Calculations for n = 100, γ = 1	A-6

1.0 INTRODUCTION AND SUMMARY

Fluctuations of signal and noise power are known to affect the performance of passive sonar systems. Prediction of the effects of fluctuations are usually based on the distribution of the signal excess, the excess of the signal-to-noise ratio required at the receiver input to achieve a detection probability of one-half. If the signal excess is broadly distributed, the detection probability is approximately

$$P_D \simeq \int_0^\infty dx\ f_E(x) \qquad (1.1)$$

where $f_E(x)$ is the probability density of the signal excess. The formulation above is based on the assumption (usually unstated) that the relaxation time of the signal excess process is very large compared to the post-rectification averaging time of the sonar receiver. A search of the underwater acoustic literature shows that in some cases the relaxation times of both signals and noise are considerably less than a nominal post-rectification averaging time of five minutes.

The directive properties of a sonar array will affect the fluctuation properties of the noise at the beamformer output. If shipping is the dominant source of noise, then the fluctuation of the noise envelope at the beamformer output will be greater the more directive the array; furthermore, the relaxation time of that noise envelope will be shorter.

This report develops a method for predicting the performance of a passive sonar operating with signals and noise with intensity envelope fluctuations with arbitrary relaxation times.

A Monte Carlo method is used that is based on a compound random process for fluctuating signals and noise, and on a multi-channel analog.

The compound random process for fluctuating noise was introduced in Reference 1 and is also described in Reference 2. This non-Gaussian process appears Gaussian for very short observation periods. This property conforms to the properties of ambient noise as determined by careful measurement and statistical analysis [3].

The multichannel analog, introduced in Reference 1, was devised as an alternative to a single-channel receiving analog consisting of an input bandpass filter, a rectifier, an averager, and a fixed threshold. In the multichannel analog, a threshold is formed by a linear combination of the outputs of a set of neighboring channels. The analog is shown to adapt to very slow changes in overall noise levels to maintain a constant false alarm probability. This performance characteristic would be achieved by a properly-designed automatic detection system or by operators viewing displays time histories of multiple inputs such as beam-former outputs.

The results of several experimental programs concerning the intensity envelopes of ambient noise and signals are reviewed. Depending on circumstances, relaxation times of signals or noise can range from much less than to much greater than a representative post-rectification averaging time of a passive sonar receiver.

Methods were developed for predicting the probability of false alarm for the case in which the inputs have a common fluctuating power envelope. An analytical method is derived for predicting the probability of false alarm for two limiting cases: very slow and very fast fluctuations. The Monte Carlo approach is used for intermediate cases. The results show that the probability of false alarm increases with the rate of noise power fluctuation as well as on the degree of fluctuation. It is shown that false alarm probabilities can be an order of magnitude greater than that predicted assuming either Gaussian noise or noise with a very slowly varying intensity envelope.

Methods were developed for predicting the probability of detection for the case of the common fluctuating power envelope. Analytical results are obtained for the case of Gaussian inputs, and for the case of very slow fluctuations, a result is obtained that can be evaluated by numerical integration. Intermediate cases are examined by a Monte Carlo simulation. It is shown that the envelope relaxation time has a very modest effect on detection differential. However, the spread of the transition curve, which gives the probability of detection as a function of input signal-to-noise power ratio, increases appreciably with the relaxation time of the power envelopes.

The case in which the noise inputs have partially-correlated noise power envelopes is examined. Analytical results are obtained for the limiting cases of very slow and very fast fluctuations, and a Monte Carlo simulation is employed for intermediate cases. In the case examined, the

envelope of the center channel had a correlation of 0.75 with either adjacent channel, one of which had a correlation of 0.5 with the other. For this case, it was found that the false alarm probability increased with the envelope relaxation time, which is opposite of the result for fully-correlated envelopes. For the limiting case of very fast envelope fluctuations, the false alarm probabilities were equal for the two cases. Thus, except for the limiting case of very fast fluctuations, the probability of false alarm for the case of partially-correlated noise envelopes is greater than that for the case of fully-correlated noise envelopes.

The Monte Carlo approach was used to generate transition curves which were found to be qualitatively similar to those obtained in the case of fully correlated noise power envelopes.

2.0 SIMULATION

The performance of a passive sonar receiver operating in an environment with highly fluctuating inputs will be predicted by simulating the receiver and its inputs by means of digital computation.

2.1 Sampled Data Multichannel Analog and Inputs

A multichannel analog for a passive sonar receiver was described in Ref. 1, which showed that the analog adapted to very slow changes of noise level to maintain a constant false alarm probability. This performance characteristic is achieved by properly-designed automatic detection systems or by operators using displays presenting time histories of multiple inputs.

Figure 2.1 shows one channel of a multichannel analog with two adjacent channels providing an adaptive offset or threshold. The value of the parameter c is selected to achieve an acceptable false alarm probability. The number of threshold channels need not be limited to two. The symbol SQ denotes squaring, RS denotes a running sum, and SI denotes a set indicator whose operation is characterized as follows:

$$\begin{aligned} D &= 1, \; Z \geq 0 \\ &= 0, \; Z < 0 \end{aligned} \qquad (2.1)$$

The operations shown in Figure 2.2 are equivalent to those shown in Figure 2.1. The former are convenient for simulation since only one running sum is required.

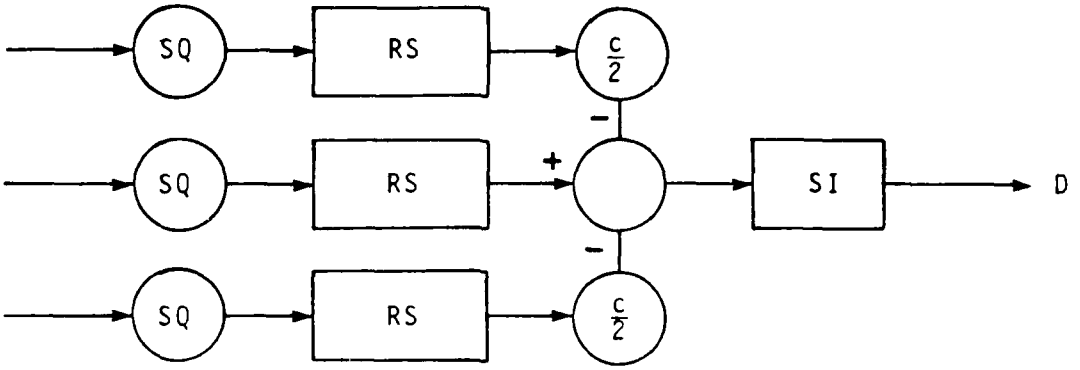

Figure 2.1 Channel with Threshold Formation

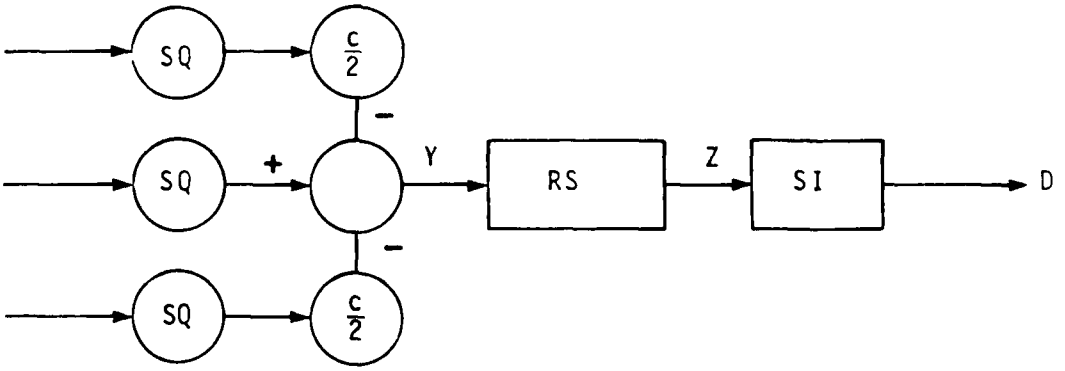

Figure 2.2 Equivalent Operations

The random process employed for characterizing the fluctuating inputs was described in Section 4.0 of Ref. 1 and in Ref. 2. In brief, the process is

$$N(t) = \sqrt{P(t)}\, G(t) \qquad (2.2)$$

where $P(t)$ is a non-negative stationary random process,
$G(t)$ is zero-mean unit variance stationary Gaussian process that is statistically independent of $P(t)$.

It is further stipulated that the relaxation time of $P(t)$, termed the power envelope, is much greater then that of $G(t)$, which then determines the bandwidth of $N(t)$. The operations involved in generating $N(t)$ from computer-generated inputs are shown in Figure 2.3.

The generation of a chi-squared envelope is straight forward; Figure 2.4 illustrates the generation of one with three degrees of freedom. The Gaussian inputs, mutually independent, are applied to identical linear lowpass filters (LPF). Possibly, the simplest case is one in which these operations are running sums (RS). In that case, the output of the RS in the ith channel at sample time j is

$$S_i(j) = \sum_{k=j-e+1}^{j} G_i(k) \qquad (2.3)$$

where $G_i(k)$ is normal (0,1) and independent of any G-variate with a different channel subscript and/or time index
e is the number of terms in the running sum.

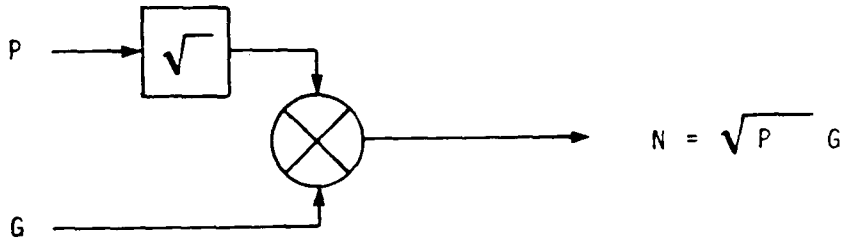

Figure 2.3 Input Generation

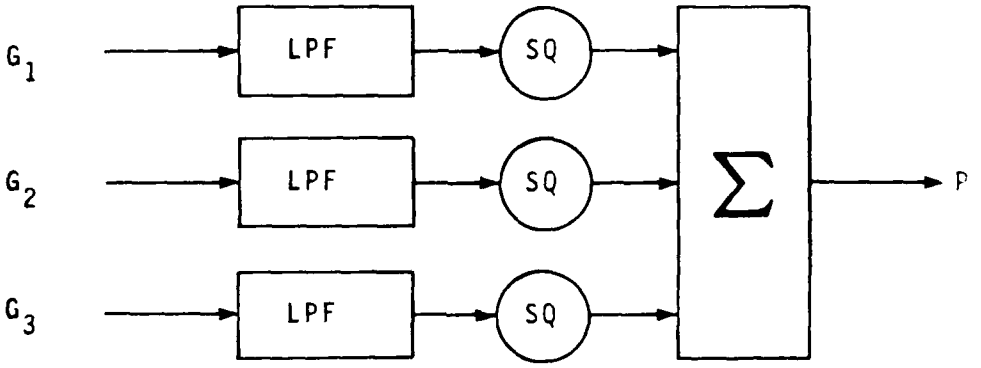

Figure 2.4 Power Envelope Formation

The covariance of $S_i(j)$ is

$$\begin{aligned} K_i(j-k) &= e - j+k, \quad 0 \leq j-k \leq e \\ &= e + j-k, \quad e \leq j-k \leq 0 \\ &= 0, \text{ otherwise} \end{aligned} \tag{2.4}$$

The output of the final summer is

$$P(j) = \sum_{i=1}^{m} S_i^2(j) \tag{2.5}$$

where m is the number of degrees of freedom. The mean value of $P(j)$ is me; thus $e^{-1}P(j)$ is chi-squared with m degrees of freedom. The covariance of $P(j)$ is

$$\begin{aligned} K_p(j-k) &= 2m\,(e-j+k)^2, \quad 0 \leq j-k \leq e \\ &= 2m\,(e+j-k)^2, \quad -e \leq j-k \leq 0 \\ &= 0, \text{ otherwise} \end{aligned} \tag{2.6}$$

In the threshold formation channels, certain operations can be simplified. Figure 2.5 shows that the output of the squarer in one of those channels is PG^2. By moving the squarer to the G input, it is possible to eliminate the square-root operation on the P input to achieve the same result, as shown in Figure 2.6.

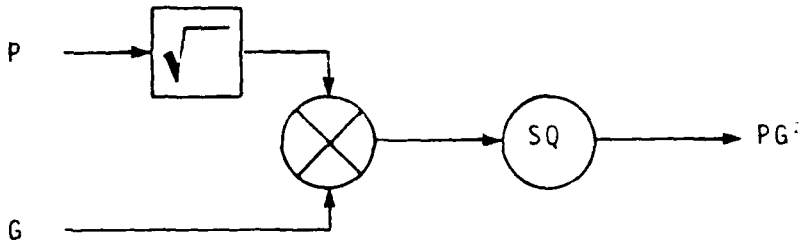

Figure 2.5 Square of Noise Input

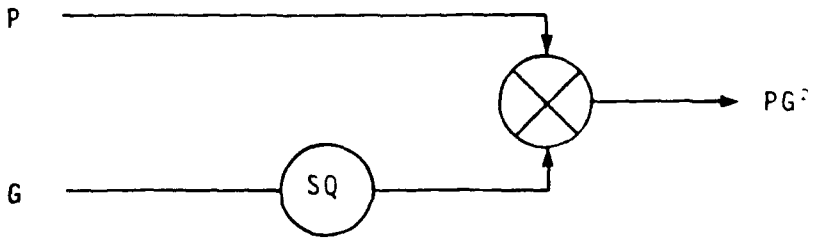

Figure 2.6 Simplified Operation

Further simplifications are possible for the case in which all channels have a common noise power envelope. Figure 2.7 illustrates the input operations for the two threshold formation channels. The result of these operations is seen to be a constant times a chi-squared variate with two degrees of freedom. One half of the latter is an exponential variate E with a mean value of one. The equivalent output is shown on the right side of Figure 2.8, which also shows the generation of this output from the inputs P and E. An exponential variate is more easily generated than a Gaussian variate.

2.2 Estimation of Probabilities

As stated previously, the output D of the analog is 1 or 0 depending on whether Z is greater than zero or not. The maximum likelihood estimator of the probability of exceeding zero is

$$\hat{p} = r^{-1} \sum_{i=1}^{r} D_i , \tag{2.7}$$

and the indicated sum is a binomial variate. The upper 95 per cent confidence limit is the value of p for which

$$\sum_{j=0}^{k} \binom{r}{j} p^j (1-p)^{r-j} = .025, \tag{2.8}$$

and the lower limit is the value of p for which

$$\sum_{j=k}^{r} \binom{r}{j} p^j (1-p)^{r-j} = .025 \tag{2.9}$$

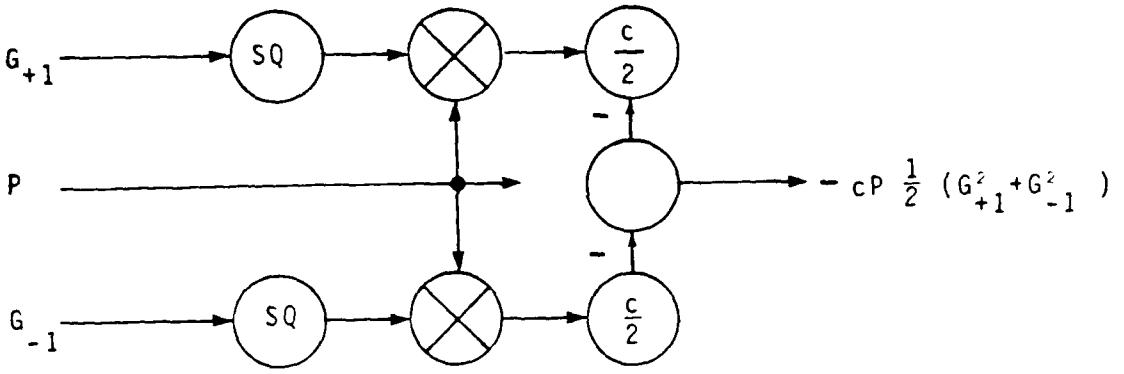

Figure 2.7 Common Noise Power Envelope

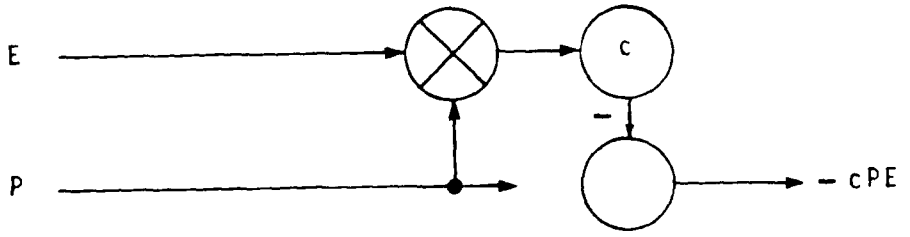

Figure 2.8 Equivalent Threshold

For determing relatively low values of false alarm probabilities, the calculation of the lower limit by the equation above would require more arithmetical operations than necessary. To arrive at a more efficient form, consider the identity

$$\sum_{j=0}^{r} \binom{r}{j} p^j (1-p)^{r-j} = 1 \qquad (2.10)$$

and subtract (2.9) from it:

$$\sum_{j=0}^{k-1} \binom{r}{j} p^j (1-p)^{r-j} = 0.975 \qquad (2.11)$$

The forms (2.8) and (2.11) are more readily calculated by recursive methods; for example, the sum in (2.8) is

$$s(p) = \sum_{j=0}^{k} T_j \qquad (2.12)$$

where $$T_j = \frac{n+1-j}{j} \cdot \frac{p}{1-p} T_{j-1}$$

$$T_0 = (1-p)^n$$

Confidence limits for selected values of $\hat{p}$ are given in Table 2.1 for r = 1000 (independent samples. Values not given in the table may be obtained by linear interpolation.

TABLE 2.1

Confidence limits for p

$\hat{p}$	p_ℓ	p_u
0	0	.0037
.001	2.53-5	.0056
.002	2.43-4	.0072
.003	6.19-4	.0087
.004	.0011	.0102
.005	.0016	.0116
.006	.0022	.0130
.007	.0028	.0144
.008	.0035	.0157
.009	.0041	.0170
.010	.0048	.0183
.015	.0084	.0246
.020	.0123	.0307
.025	.0162	.0367
.030	.0203	.0425
.040	.0287	.0541
.050	.0373	.0654
.060	.0461	.0766
.070	.0550	.0877
.080	.0639	.0986
.090	.0730	.1095
.100	.0821	.1203

When the product p(1-p)r is large (here p is the number of trials), the 95 per cent confidence limits are given approximately by

$$p_\ell = \hat{p} - \delta \tag{2.13}$$

$$p_u = \hat{p} + \delta \tag{2.14}$$

where $\delta = 1.96 \sqrt{\frac{\hat{p}(1-\hat{p})}{r}}$

For $\hat{p} = 0.1$ and $r = 1000$, then $\hat{p}(1-\hat{p})r = 90$, $\delta = .0186$, $p_\ell \approx .0814$, and $p_u \approx .1186$. The corresponding limits from Table 2.1 are $p_\ell = .0821$ and .1203. Thus for r= 1000 and $\hat{p} \geq 0.1$, the accuracy of the approximate limits is satisfactory.

The confidence interval $p_u - p_\ell$ is maximum for $\hat{p} = 0.5$, and it decreases with a decrease of $\hat{p}$. However, the ratio of the length of the confidence interval to the value of the estimator increases with a decrease of $\hat{p}$. From (2.13) and (2.14) we obtain

$$\frac{1}{2} \cdot \frac{p_u - p_\ell}{p} \approx \frac{\delta}{\hat{p}} = 1.96 \sqrt{\frac{1-\hat{p}}{r\hat{p}}} \tag{2.15}$$

For r = 1000 and $\hat{p} = 0.9$, $\delta/\hat{p} = .02$, and for $\hat{p} = 0.1$, $\delta/\hat{p} = 19$; thus, for estimating detection probabilities between 0.1 and 0.9, sufficient accuracy obtains using 1000 independent samples. The corresponding number of input samples required in 1000 (e+n), where e is the number of terms in the running sum of the

multichannel analog. If n = 60, and if the maximum value of e is 60, then 120,000 independent input samples are required.

For the estimation of false alarm probabilities, the requirements are more stringent. For $\hat{p} = .01$ and $r = 1000$, we obtain from Table 2.1 $\delta/\hat{p} = 0.67$, which is not very good, but possibly acceptable. For $\hat{p} = .001$, the lower and upper limits are $2.5 \times 10^{-\delta}$ and .0056 respectively, which for most purposes would be unsatisfactory. Thus for the estimation of low false alarm probabilities, a much greater number of samples will be required.

3.0 SPECIAL CASE: GAUSSIAN NOISE INPUTS

3.1 Introduction

The special case of homogeneous stationary Gaussian noise inputs is of interest for two reasons: the results of an analysis of this case will serve to check certain results of the simulation and to show the convergence of the output of the sampled data multichannel analog to first-order normality. The assumption of normality conditioned on the power envelope will be used to derive results in subsequent sections for limiting cases of both slow and fast fluctuations.

Results of this section include low-order central moments, skewness, kurtosis, the probability density function of the output, and the probability of false alarm.

For the special case of Gaussian noise inputs, the output of the sampled-data multichannel analog may be expressed as

$$Z = \sum_{i=1}^{n} \left(p_o G_{oi}^2 - \frac{c}{m} \sum_{j=1}^{m} p_j \, G_{ji}^2 \right) \qquad (3.1)$$

where p_j is the average power of the input to channel j,

G_{ji} is a zero-mean unit-variance normal random variate, statistically independent of the other random variates with a different subscript. The subscript j denotes channel numbers and the subscript i denotes the sample frame.

c is a non-negative constant whose value affects the false alarm probability

n is the number of samples in the running sums,

m is the number of channels used for forming the threshold for channel 0.

In this context, the term homogeneous noise implies that the average noise power in each channel is the same. For this case, the output can be expressed as

$$Z = pQ \tag{3.2}$$

where p is the average noise power of each channel

$$Q = Y - \frac{c}{m} X \tag{3.3}$$

Y is a chi-squared random variable with n degrees of freedom,

X is a chi-squared random variable with mn degrees of freedom.

The probability density of Z can be expressed in terms of the probability density of Q:

$$f_Z(z) = p^{-1} f_Q(zp^{-1}) \tag{3.4}$$

Furthermore, the moments of Z can be expressed in terms of the moments of Q:

$$m_{iP} = p^i m_{iQ} \tag{3.5}$$

In the sequel, the basic analyses concern the normalized variable Q, and the results are extended to the variate Z via (3.4) or (3.5) as appropriate.

3.2 Skewness and Kurtosis

The principal objective of this analysis is to obtain a quantitative measure of the non-normality of the output. The analysis is entirely straightforward and is based on the chi-squared moments formula given in Ref. 4.

The mean value of Q and the second through fourth central moments are

$$m_Q = n(1-c) \tag{3.6}$$

$$\sigma_Q^2 = \mu_{2Q} = 2n(1+c^2/m) \tag{3.7}$$

$$\mu_{3Q} = 8n\,(1-c^3/m^2) \tag{3.8}$$

$$\mu_{4Q} = 12n[(1+c^2/m)^2 n + 4(1+c^4/m^3)] \tag{3.9}$$

Note that the variance of Q increases with the value of c, the threshold parameter.

The skewness is obtained by dividing μ_{3Q} by σ_Q^3:

$$s_Q = 2\sqrt{\frac{2}{n}}\, f(c) \tag{3.10}$$

where $$f(c) = \frac{1-c^3/m^2}{(1+c^2/m)^{3/2}}$$

Salient features of the function f(c) are presented in Table 2.1

TABLE 3.1

Salient Features of f(c)

c	$-\infty$	$-m$	0	$m^{2/3}$	∞
f(c)	$1/\sqrt{m}$	$1/\sqrt{m+1}$	1	0	$-1/\sqrt{m}$
comment	assymptotic	minimum	maximum	zero	assymptotic

The case c = 0 corresponds to a single-channel analog; at this point, the function f(c) achieves a global as well as a local maximum. If $m > 1$, the function achieves a global absolute maximum. Although it is of no practical importance, the minimum at $c = m$ corresponds to an output with $n(m+1)$ degrees of freedom.

The kurtosis is obtained by dividing μ_{4Q} by σ_Q^4, and the deviation of the kurtosis from the value three for a normal random variate is

$$\delta_Q = \frac{12}{n} g(c) \qquad (3.11)$$

where $g(c) = \dfrac{1+c^4/m^3}{(1+c^2/m)^2}$

The function g(c) has even symmetry, and its salient features are shown in Table 2.2.

TABLE 3.2

Salient Features of g(c)

c	0	$\pm m$	$\pm\infty$
g(c)	1	$1/(1+m)$	$1/m$
comment	maximum	minimum	assymptotic

Again, the maximum at zero is global for $m > 1$.

Thus, according to the measures of skewness and kurtosis, the normalized output of the multichannel analog is more Gaussian than that of the single-channel analog if $m > 1$, where m is the number of channels employed for threshold formation. Since the moments of the output Z are proportional to those of Q, they have the same skewness and kurtosis.

3.3 Probability Density

The probability density of the normalized output will be derived from expressions for its distribution function. The distribution of Q is

$$F_Q(q) = P(Q \leq q), \tag{3.12}$$

and substituting (3.3) in 3.12) gives

$$F_Q(q) = P(Y - \frac{c}{m}X \leq q) \tag{3.13}$$

Since X and Y are each derived from independent sets of variates, their joint density is the product of their individual densities.

For $q \geq 0$, the distribution is

$$F_Q(q) = \int_0^\infty dx\ f_X(x) \int_0^{q+\frac{c}{m}x} dy\ f_Y(y) \quad , \tag{3.14}$$

and the probability density is

$$f_Q(q) = \frac{\partial}{\partial q} F_Q(q)$$

$$= \int_0^\infty dx\ f_X(x) f_Y(z+\frac{c}{m}x) \tag{3.15}$$

If the appropriate chi-squared densities are substituted in (3.15), an integral is obtained tha can be evaluated by 3.351 No. 3 of Ref. 5 for cases in which n is an even number, and the result obtained is

$$f_Q(q) = (\frac{m}{m+c})^{\frac{mn}{2}} \frac{e^{-q/2}}{2} \sum_{k=}^{\frac{n}{2}-1} \frac{[(1+m)\frac{n}{2} - 2 - k]!}{(\frac{mn}{2}-1)!(\frac{n}{2}-1-k)!} (\frac{c}{m+c})^{\frac{n}{2}-1-k} \frac{(q/2)^k}{k!}, \quad q \geq$$

For $q \leq 0$, the distribution is given by

$$F_Q(q) = \int^\infty dy\ f_Y(y) \int_{\frac{m}{c}(y-z)}^\infty dx\ f_x(x) \tag{3.17}$$

Since X and Y are each derived from independent sets of variates, their joint density is the product of their individual densities.

For $q \geq 0$, the distribution is

$$F_Q(q) = \int_0^\infty dx\ f_X(x) \int_0^{q+\frac{c}{m}x} dy\ f_Y(y) \quad , \tag{3.14}$$

and the probability density is

$$f_Q(q) = \frac{\partial}{\partial q} F_Q(q)$$

$$= \int_0^\infty dx\ f_X(x) f_Y(z+\frac{c}{m}x) \tag{3.15}$$

If the appropriate chi-squared densities are substituted in (3.15), an integral is obtained tha can be evaluated by 3.351 No. 3 of Ref. 5 for cases in which n is an even number, and the result obtained is

$$f_Q(q) = (\frac{m}{m+c})^{\frac{mn}{2}} \frac{e^{-q/2}}{2} \sum_{k=}^{\frac{n}{2}-1} \frac{[(1+m)\frac{}{2} - 2 - k]!}{(\frac{m}{2}-1)!(\frac{n}{2}-1-k)!} (\frac{c}{m+c})^{\frac{n}{2}-1-k} \frac{(q/2)^k}{k!}, \quad q \geq 0$$

For $q \leq 0$, the distribution is given by

$$F_Q(q) = \int^\infty dy\ f_Y(y) \int_{\frac{m}{c}(y-z)}^\infty dx\ f_X(x) \tag{3.17}$$

and the density is given by

$$f_Q(q) = \int_0^\infty dy\, f_Y(y)\, f_X\left[\frac{m}{c}(y-z)\right] \qquad (3.18)$$

If the appropriate chi-squared densities are substituted in (3.18), an integral is obtained that can be evaluated by 3.351 No. 3 of Ref. 5 for cases in which n is an even number. The result obtained is

$$f_Q(q) = \left(\frac{m}{c+m}\right)^{\frac{mn}{2}} \frac{e^{\frac{mq}{2c}}}{2} \sum_{k=0}^{\frac{mn}{2}-1} \frac{[(1+m)\frac{n}{2} - 2 - k]!}{(\frac{mn}{2}-1-k)!(\frac{n}{2}-1)!} \left(\frac{c}{c+m}\right)^{\frac{n}{2}-1-k} \frac{(-q/2)^k}{k!}, \quad q \le 0 \qquad (3.19)$$

To the purpose of calculations, it is useful to calculate the coefficients by means of recursion formulas. The results can be summarized as follows:

$$\begin{aligned} f_Q(q) &= e^{\frac{m}{c}\cdot\frac{q}{2}} \sum_{k=0}^{\frac{mn}{2}-1} P_k(q) \quad , \quad q < 0 \\ &= P_k(0) \quad , \quad q = 0 \\ &= e^{-q/2} \sum_{k=0}^{\frac{n}{2}-1} Q_k(q) \quad , \quad q > 0 \end{aligned} \qquad (3.20)$$

where

$$P_k(q) = \frac{(\frac{mn}{2}-k)}{[(1+m)\frac{n}{2}-1-k]k} \left(\frac{c}{c+m}\right)^{-1} \frac{-q}{2} P_{k-1}(q) \qquad (3.21)$$

$$Q_k(q) = \frac{(\frac{n}{2}-k)}{[(1+m)\frac{n}{2}-1-k]k} \left(\frac{c}{c+m}\right)^{-1} \frac{q}{2} Q_{k-1}(q) \qquad (3.22)$$

$$P_o(q) = Q_o(q) = \frac{1}{2}\left[\prod_{i=1}^{\frac{n}{2}-1} \left(\frac{n-1+i}{i}\right)\right] \left(\frac{m}{m+c}\right)^{\frac{mn}{2}} \left(\frac{c}{c+m}\right)^{\frac{n}{2}-1} \qquad (3.23)$$

These results are valid only when n is an even number.

Figure 3.1 through 3.4 show the density of Q for various values of n, the number of terms in the running sum, and c, the threshold parameter. The number m of threshold channels is two. To show the departure from normality, normal curves with the same mean and variance are also plotted. These functions are given by

$$f_A(z) = \frac{Z\left(\frac{z+n(c-1)}{\sqrt{2n(1+c^2/m}}\right)}{\sqrt{2n(1+c^2/m)}} \qquad (3.24)$$

where Z( ) is the normal density function for zero mean and unit variance.

Table 3.3 gives low-order moments and measures for the same combinations of parameter values. Even for n = 6, the deviation from normal is not extreme; however, the convergence is slow, and the deviation is still apparent for n = 60.

TABLE 3.3

Measures and Moments

n	6	6	14	14	30	30	60	60
c	1.0	1.5	1.0	1.4	1.0	1.3	1.0	1.2
m_Q	0	-3.0	0	-5.6	0	-9.0	0	-12.0
σ_Q	4.24	5.05	6.48	7.45	9.49	10.5	13.4	14.4
s_Q	0.47	.06	0.31	.09	0.21	.09	.15	.09
δ_Q	1.0	.72	0.43	.32	0.20	.16	.10	.09

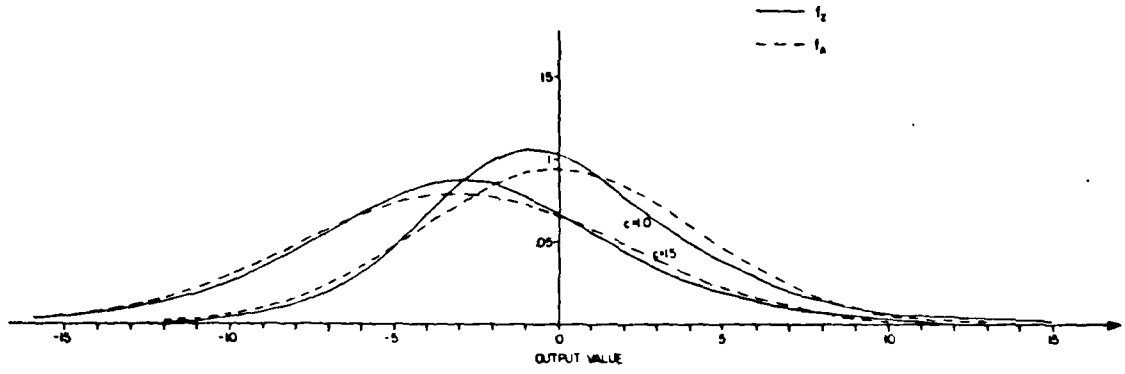

FIGURE 3.1 Density of Output for n = 6

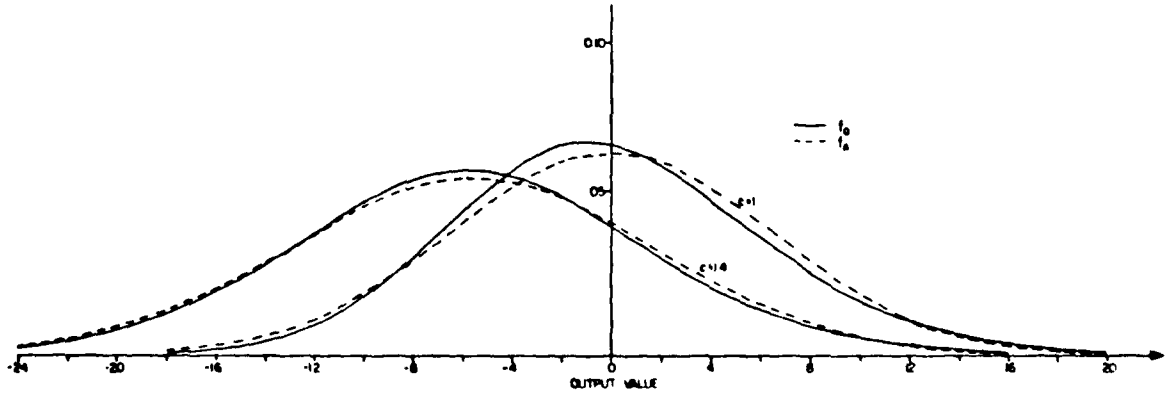

FIGURE 3.2 Density of Output for n = 14

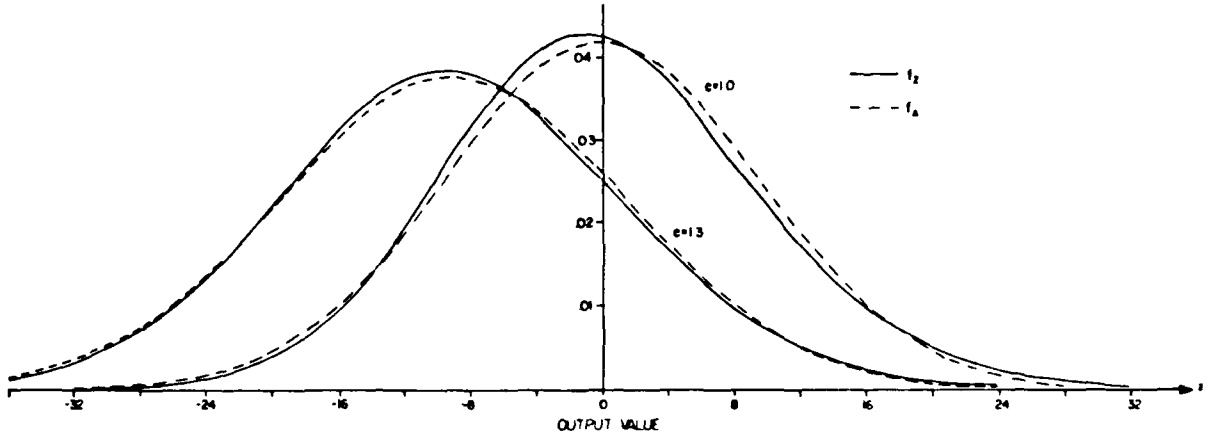

FIGURE 3.3 Density of Output for n = 30

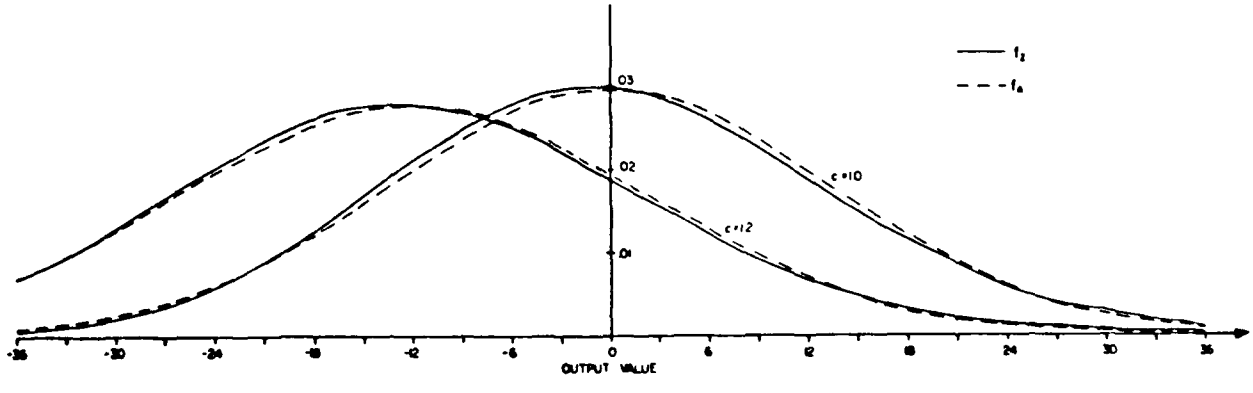

FIGURE 3.4 Density of Output for n = 60

3.4 False Alarm Probability

The false alarm probability is

$$P_F = P(Z > 0|\bar{S}) = \int_0^\infty dz\, f_Z(z|\bar{S}) \tag{3.25}$$

where $\bar{S}$ denotes that no signal is present.

Substituting (3.4) in (3.25) gives

$$P_F = p^{-1} \int_0^\infty dz\, f_q(zp^{-1}) \tag{3.26}$$

A change of variable $x = zp^{-1}$ gives

$$P_F = \int_0^\infty dz f_Q(z)\ , \tag{3.27}$$

which shows that the false alarm probability is independent of the average input power.

Substituting (3.16) in (3.27) yields a form that can be integrated using 3.351 No. 2 of Ref. 5. Then if the summation index is changed to $j = n/2-1-k$ the result is

$$P_F = \left(\frac{m}{m+c}\right)^{\frac{mn}{2}} \sum_{j=0}^{\frac{n}{2}-1} \frac{(\frac{mn}{2}-1+k)!}{(\frac{mn}{2}-1)!k!} \left(\frac{c}{m+c}\right)^j \tag{3.28}$$

$$= \sum_{j=0}^{\frac{n}{2}-1} R_j \tag{3.29}$$

$$R_j = \frac{\frac{mn}{2}-1+k}{k} \frac{c}{m+c} R_{j-1}\ ,\ j \geq 1 \tag{3.30}$$

$$R_0 = \left(\frac{m}{m+c}\right)^{\frac{mn}{2}} \tag{3.31}$$

If the analog output is assumed to be normal, then the false alarm probability is

$$P_A = Q\left(\frac{n(c-1)}{\sqrt{2n(1+c^2/m)}}\right) \qquad (3.32)$$

where $Q(x) = \int_x^\infty du\ Z(u)$

Figures 3.5 through 3.8 show the false alarm probability of the sampled-data multichannel analog as a function of the threshold parameter C. Also shown is the false alarm probability calculated assuming a normal output. The sequence shows, as expected, that the approximation improves with n, the number of terms in the past-rectification running sum. Or, put another way, it shows the convergence of the output density to normal.

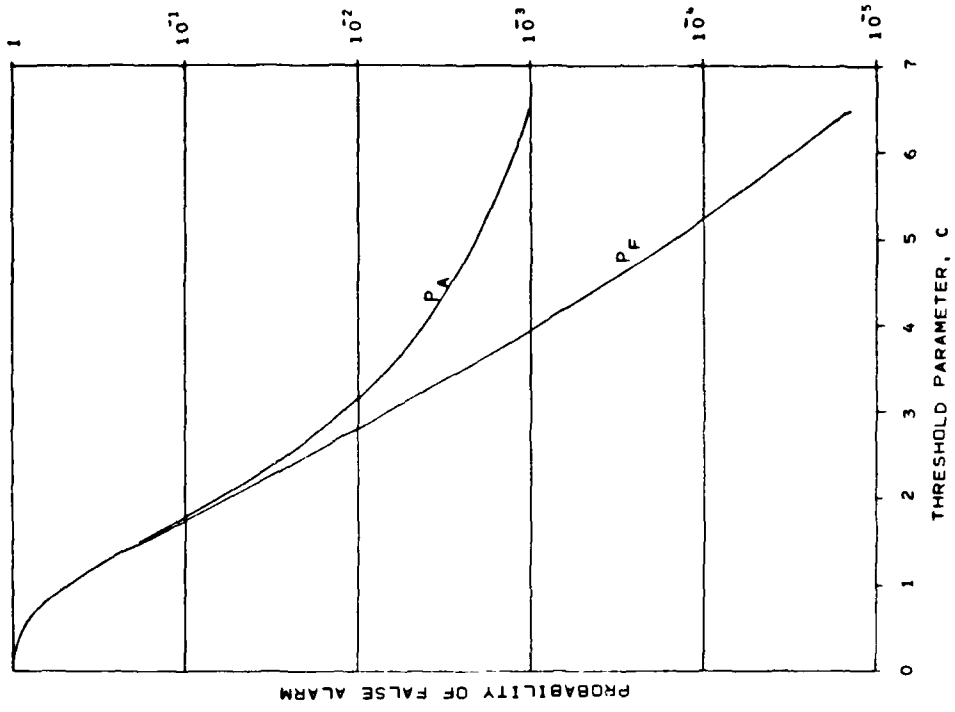

FIGURE 3.6 P_F and P_A for n = 14
m = 2

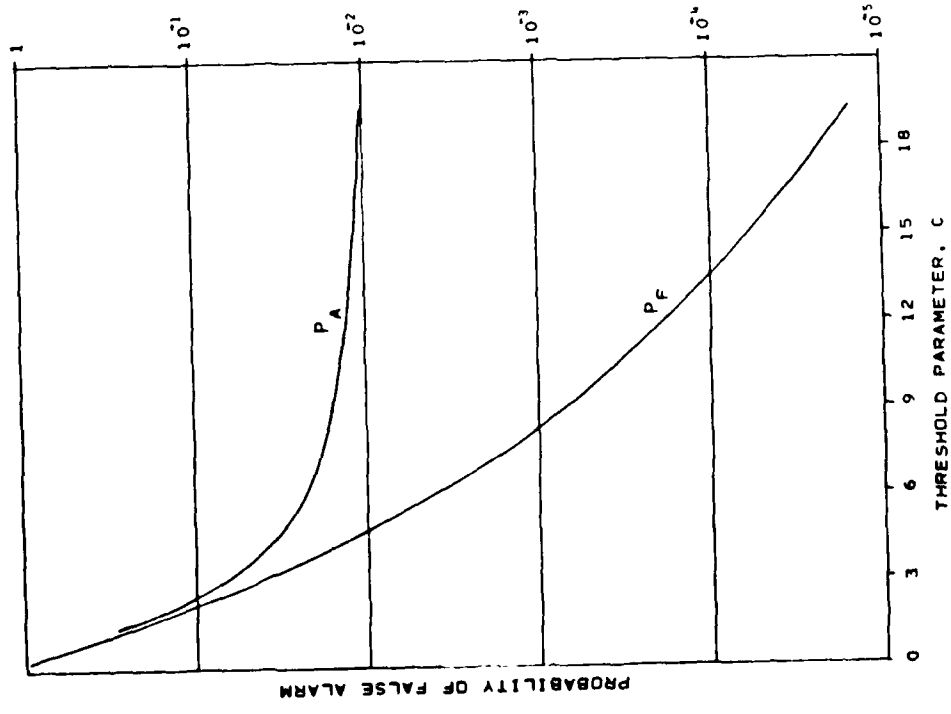

FIGURE 3.5 P_F and P_A for n = 6
m = 2

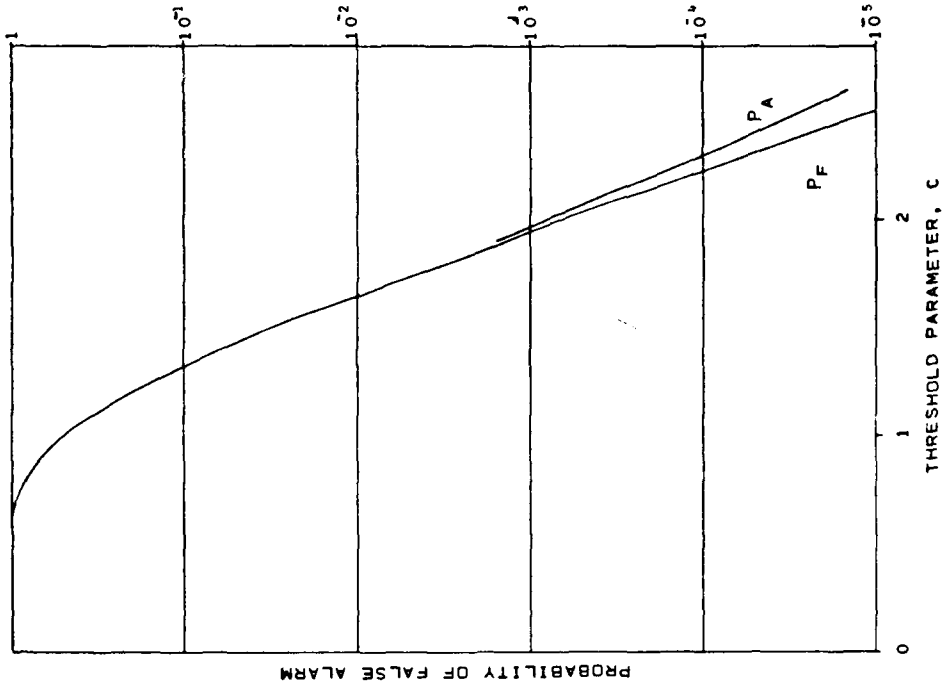

FIGURE 3.8 P_F and P_A for n = 60
m = 2

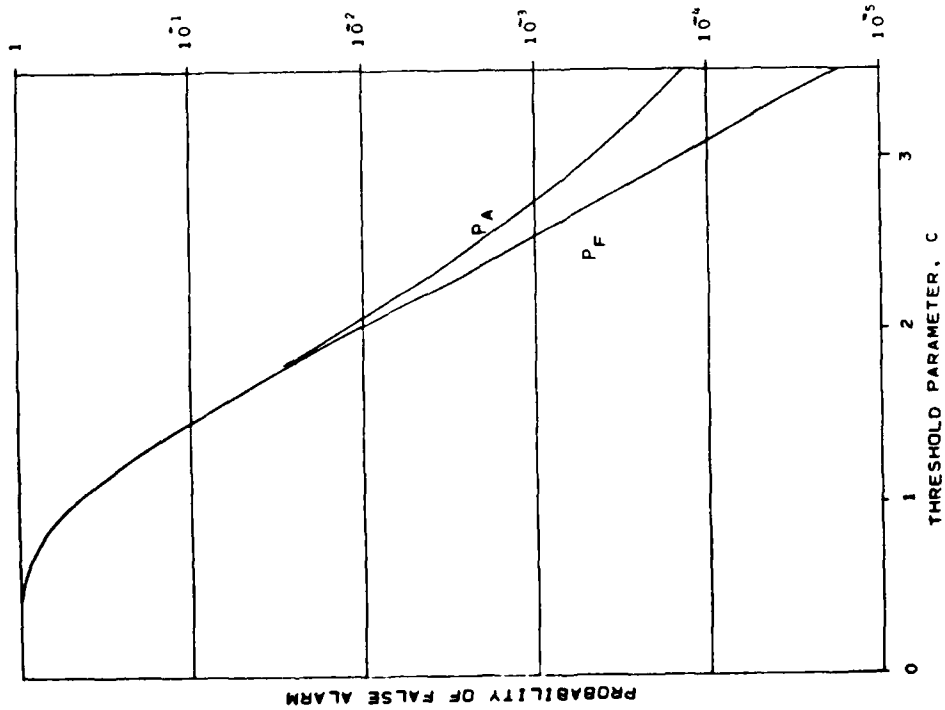

FIGURE 3.7 P_F and P_A for n = 30
m = 2

4.0 NOISE AND SIGNAL CHARACTERIZATION

4.1 Introduction

The results of numerous experiments show that underwater ambient (acoustic) noise cannot be represented by a stationary Gaussian process. Most of these experiments concern the squared pressure averaged over a period of time on the order of a minute. The excessive variance of that quantity (or ten times the logarithm of that quantity to the base ten) shows that the noise pressure does not have stationary Gaussian characteristics. This conclusion is also supported by a much smaller number of experiments that concern the statistics of the noise pressure itself. These experiments provide the additional information that the noise pressure exhibits nearly Gaussian characteristics for short observation periods.

A stochastic process displaying the characteristics described above is easily evolved. First define G(t) as a stationary Gaussian process with zero mean and unit variance. Next multiply it by $\sqrt{v}$, $v>0$; the result is a stationary Gaussian process with zero mean and variance v. Instead, multiply G(t) by $\sqrt{V}$, where V is a non-negative random variable statistically independent of G(t). This is a zero-mean non-Gaussian process called a compound Gaussian process that has been studied and applied [6,7]. Given a realization of V, the process is conditionally a stationary zero-mean Gaussian process. This process does not have the characteristics described in the previous paragraph because a sample function of the process has stationary Gaussian characteristics regardless of the period of observation. For the final step of the evolution, multiply G(t) by $\sqrt{V(t)}$, where V(t) is a non-negative random process independent of G(t).

The result is again a zero-mean non-Gaussian process. It is stationary if V(t) is stationary, and vice versa. Now suppose that an observation period T_0 can be found such that

$$T_V >> T_0 >> T_G \tag{4.1}$$

where T_V is the relaxation time of the V-process

T_G is the relaxation time of the G-process.

Then during the observation period, a sample function of the V-process will vary hardly at all, and a sample function of the G-process will go through many alternations. Thus, the sample function will exhibit nearly Gaussian characteristics during a period of observation period satisfying (4.1). Arase and Arase [3] found that sample functions of ambient noise pressure satisfied stationary Gaussian criteria more often with 10-second observation periods than with periods of 20 and 40 seconds.

For the most general representation, the V-process would be nonstationary because the phenomena that generate and propagate sound may have annual, lunar, or diurnal dependencies. However, if the period of interest is very small compared to the period of the shortest cycle, then the process, with suitable selection of parameters, can be assumed to be locally stationary. For example, the post-rectification averaging time of a passive sonar is very small compared to this diurnal period.

The probability density function for the compound process

$$N(t) = \sqrt{V(t)}\, G(t)^{*}$$

may be found from its conditional density given V(t), which is Gaussian:

$$f_N\,[x|V(t) = v(t)] = \frac{1}{\sqrt{2\pi v(t)}} \exp -\frac{1}{2}\frac{x^2}{V(t)} \qquad (4.2)$$

The joint density of N(t) and V(t) is

$$f_{NV}(x,v;t) = f_N[x|V(t) = v(t)]\, f_V(v;t)\,, \qquad (4.3)$$

and the marginal density of N(t) is

$$f_N(x;t) = \int_{-\infty}^{\infty} dv\, f_V(v;t)\, f_N[x|V(t) = v(t)] \qquad (4.4)$$

Substituting (4.2) in (4.4) gives

$$f_N(x;t) = \int_{-\infty}^{\infty} dv\, f_P(v,t) \frac{1}{\sqrt{2\pi v}} \exp -\frac{1}{2}\frac{x^2}{v} \qquad (4.5)$$

A change of variable $v = y^2$ gives the alternative form (4.6) of [1].

The compound process $N(t) = \sqrt{V(t)}\, G(t)$ has been described previously [1,2]. Another stochastic process has been proposed [8] for arctic ambient noise: $\sqrt{v}\, G(t) + I(t)$, where the first term is stationary Gaussian noise, zero mean and variance V, and I(t) is an impulsive monstationary stochastic process. In the cited reference, the statistical properties of the

* In other sections of this report, V(t) is denoted by P(t).

proposed process were not elaborated. Certain statistical properties of N(t), previously derived, are summarized below.

The first-order moments can be obtained by substituting (4.5) in

$$m_{iN}(t) = \int_{-\infty}^{\infty} dx\ f_N(x;t) \quad , \tag{4.6}$$

or, perhaps more easily from

$$m_{iN}(t) = E[V^{i/2}(t)]\ E]G^i(t)]. \tag{4.7}$$

The moments of the standardized Gaussian variate are well known; thus

$$\begin{aligned} m_{iN}(t) &= 0, \ i \ \text{odd} \\ &= m_{\frac{i}{2}V}\ \frac{i!}{(\frac{i}{2})!\ 2^{i/2}} \ , \ i \ \text{even} \end{aligned} \tag{4.8}$$

The mean value is zero, as would be expected for either a bandpass or highpass process; this was also demonstrated experimentally [9]. Since the mean value is zero, all moments are central moments. The skewness coefficient s_N, defined as $\mu_{3N} \div \sigma_N^3$, is zero.

The kurtosis is

$$k_N \equiv \frac{\mu_{4N}}{\sigma_N^4} = \frac{3m_{2V}}{m_V^2} = 3\,\frac{m_V^2 + \sigma_V^2}{m_V^2} = 3\,(1 + \frac{\sigma_V^2}{m_V^2}) > 3 \tag{4.9}$$

The values of s_N and k_N are consistent with experimental results reported in (3) and discussed in (1 and 2).

Consider the second-order properties of N(t) for the cases in which V(t) is a stationary process. The covariance of N(t) is

$$K_N(\tau) = E\left[\sqrt{V(t)\,V(t+\tau)}\right]\; E\left[G(t)\,G(t+\tau)\right] . \tag{4.10}$$

If $T_V >> T_G$, then the second factor decays much more rapidly with τ than does the first, and

$$K_N(\tau) \simeq m_V \rho_G(\tau), \tag{4.11}$$

where $m_V = E[V(t)]$

$\rho_G(\tau) = E[G(t)\,G(t+\tau)]$

Now let $Q(t) = N(t)$; then

$$K_Q(\tau) \triangleq E\left[Q(t)\,Q(t+\tau)\right]$$

$$= \left[1 + 2\rho_G^2(\tau)\right] K_V(\tau) + 2\left[m_V \rho_G(\tau)\right]^2 \tag{4.12}$$

$$\simeq K_V(\tau) \quad , \quad \tau >> T_G \tag{4.13}$$

Note that the presence of the V-process is evident from $K_Q(\tau)$, but not from $K_N(\tau)$, given $T_V >> T_G$.

If an estimate of $K_N(\tau)$ is derived from measurements, then from (4.11)

$$\hat{m}_V = \hat{K}_N(0) \tag{4.14}$$

$$\hat{\rho}_G(\tau) \simeq \hat{K}_N(\tau)/\hat{K}_N(0) \tag{4.15}$$

And if an estimate of $K_Q(\ )$ is also obtained, then use of (4.12), (4.14), and (4.15) yields

$$\hat{K}_V(\tau) = \hat{K}_N^2(0) \frac{\hat{K}_Q(\tau) - 2\hat{K}_N(\tau)}{\hat{K}_N^2(0) + 2\hat{K}_N^2(\tau)} \tag{4.16}$$

That is the pair of covariance functions $K_N(\tau)$ and $K_Q(\tau)$ specifies the component process V(t) and G(t) to the second order, given $T_V >> T_G$.

To this point, only two specifications were placed on the V-process: $V(t) \geq 0$, and $T_V >> T_G$. A normalized chi-squared process has been proposed for the V-process [1,2]:

$$V(t) = m_V n^{-1} \sum_{i=1}^{n} G_i^2(t) \tag{4.17}$$

where $m_V > 0$

$G_i(t)$ is stationary Gauss $[0, r(\tau)]$, $r(0) = 1$, independent of $G(t)$ and $G_j(t)$, $i \neq j$

The covariance function of V(t) is

$$K_V(\tau) = 2m_V^2 n^{-1} r^2(\tau) \qquad (4.18)$$

Given that an estimate of $K_V(\ )$ is available as discussed in the previous paragraph, then (4.18) and (4.14) give

$$\hat{n} = 2\hat{K}_N^2(0)/K_V(0) \qquad (4.19)$$

from which the nearest integer value would be selected. And substituting (4.19) and (4.14) in (4.18) and solving gives

$$\hat{r}^2(\tau) = \hat{K}_V(\tau)/\hat{K}_V(0) \qquad (4.20)$$

Equations (4.14) through (4.20) show that the pair of factor processes are completely specified by the pair of covariance functions $K_N(\tau)$ and $K_Q(\tau)$. If N(t) were a Gaussian process, only $K_N(\tau)$ would be required for its specification.

A search of the literature has not revealed any joint estimates of $K_N(\tau)$ and $K_Q(\tau)$.

4.2 Envelope Estimation

The square of the compound process is

$$Q(t) \triangleq N^2(t) = V(t)\, G^2(t) \qquad (4.21)$$

Given that $T_V >> T_G$, then it seems reasonable to call V(t) the intensity envelope, or merely the envelope. If Q(t) is

is passed through a lowpass filter, then the result can be a good estimate of the sample function of V(t). As stated in the introduction, most ambient noise experiments concern the squared pressure averaged over a period of time on the order of a minute. The resulting time series can be sampled, and the samples can be employed to obtain estimates of the statistical parameters of the envelope. The most popular statistic is the mean value. Greater effort is required to estimate its variance, or its probability distribution, or either its covariance or power spectrum.

Estimates of the amplitude (not intensity) envelope power spectrum have been obtained for a planar array with 720 directional elements [10]. Two one-octave bands were processed: 800 - 1600 Hz and 1600 - 3200 Hz. A total of 1500 beams are DIMUS formed to cover a wide sector of azimuth and elevation angles between plus and minus 90 degrees.

The amplitude envelope power spectra for the two one-octave bands are shown in Figure 4.1 for a nearly horizontal beam. The peak above 30 mHz is attributed to an oscillation of the array. The initial negative slope is about 8 dB per octave. It is considered inadvisable to obtain an estimate of the autocovariance function by Fourier transforming the power spectrum. However, to get some idea of the temporal implication of this data, assume a first-order Butterworth spectrum (-6 dB per octave). The -3 dB frequency f_o is seen to be about 6 mHz, and the associated relaxation time is $d = (2 f_o)^{-1} \approx 26$ sec. The relaxation time of the intensity envelope (amplitude squared) is half of that, or about 13 sec.

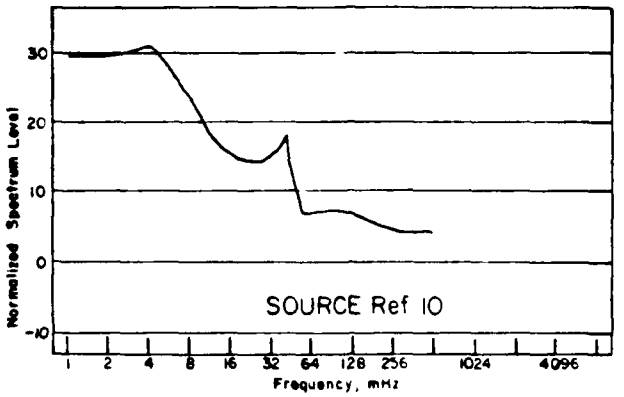

FIGURE 4.1(a) Low-band Envelope Spectrum--
Nearly Horizontal Elevation

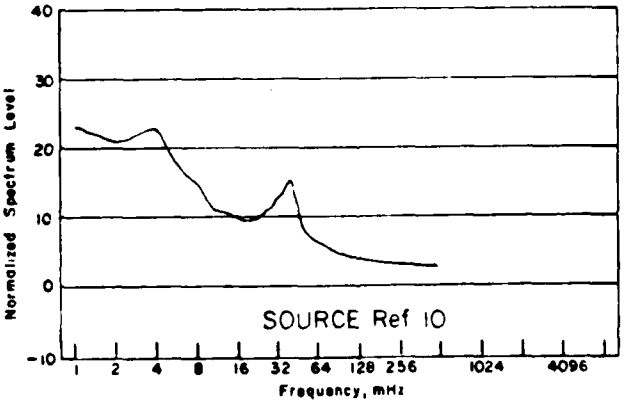

FIGURE 4.1(b) High-Band Spectrum of a
Nearly Horizontal Elevation

Figure 4.2 shows the amplitude envelope power spectra in the two one-octave bands for a beam directed at the sea surface. Here the peak in the vicinity of 100 hZ was attributed to the 8- to 10 second period wave spectral peak of the wind-generated surface waves. Finally, Figure 4.3 shows the intensity envelope power spectra in the two one-octave bands for the output of a single (directional) element. Here the energy is concentrated at lower frequencies, as expected.

For the multichannel analog, the noise input may be represented by a vector random process

$$N_i(t) = \sqrt{V_i(t)}\, G_i(t) \;,\; i = 1,2,3,\ldots,\, n \qquad (4.22)$$

where $V_i(t)$ is a non-negative stationary random process with average value m_i.

$G_i(t)$ is a zero-mean, unit variance stationary Gaussian process statistically independent of $V_j(t)$, $j = 1,2,3,\ldots,\, n$.

Now define $Q_i(t) = N_i(t)$; then the joint second moment function is

$$M_{Qij}(\tau) \triangleq E[Q_i(t)\, Q_j(t+\tau)]$$

$$= [m_i m_j + K_{Vij}(\tau)]\,[1 + 2\rho^2_{Gij}(\tau)] \qquad (4.23)$$

and the joint covariance is

$$K_{Qij}(\tau) = K_{Vij}(\tau) + 2[m_i m_j + K_{Vij}(\tau)]\,\rho^2_{Gij}(\tau) \qquad (4.24)$$

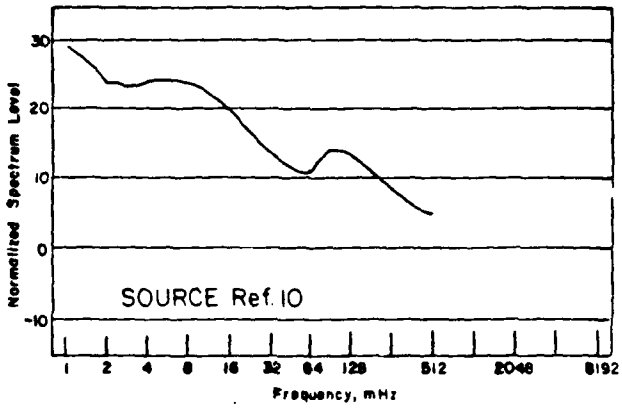

FIGURE 4.2(a) Low-Band Envelope Spectrum-Overhead Elevation

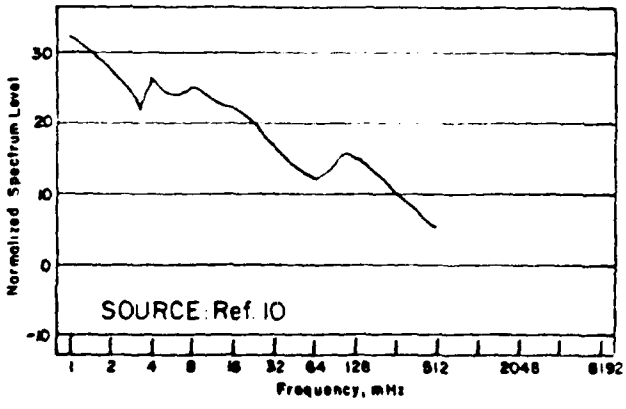

FIGURE 4.2(b) High-Band Envelope Spectrum of the Overhead Elevation

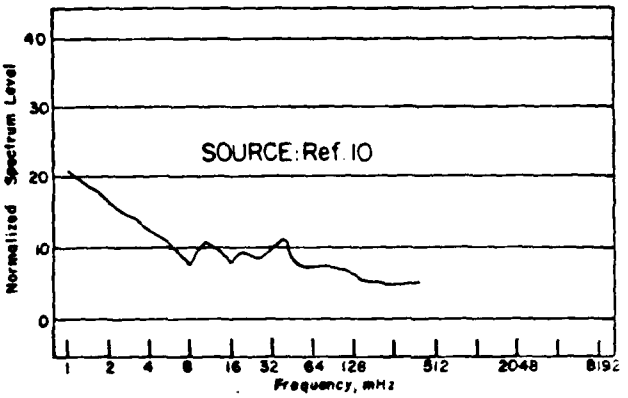

FIGURE 4.3(a) Low-Band Envelope Spectrum-Single Element

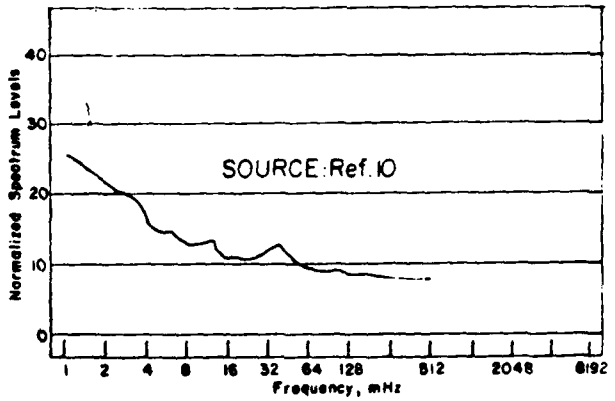

FIGURE 4.3(b) High-Band Envelope Spectrum of a Single Element

Assuming that $T_{Vi} >> T_{Gj}$, all i and all j, and that $Q_i(t)$ and $Q_j(t)$ are subjected to lowpass filtering, then

$$K_{Vij}(\tau) \approx K_{\tilde{Q}ij}(\tau) \tag{4.25}$$

where the tilde denotes lowpass filtering. Nichols, Young, and Sayer [11] obtained estimates of the normalized joint covariance of the intensity envelopes of pairs of beams; i.e., of

$$\hat{r}_{ij} = \frac{\hat{K}_{Vij}(0)}{\sqrt{\hat{K}_{Vi}(0)\,\hat{K}_{Vj}(0)}} \tag{4.26}$$

The data were derived from a bottomed linear array operating in a six Hz band dominated by shipping noise. Adjacent beams overlap at -3 dB response levels. In the azimuth sector with heavy ship traffic, $\hat{r}_{ij}$ decreases quite rapidly with $|i-j|$, where as in the azimuth sector with low ship traffic, $\hat{r}_{ij}$ decreases rather slowly with $|i-j|$. Because of their security classification, the experimental results are not summarized herein.

The characteristics of received signals are usually obtained by transmitting signals at one point and observing their characteristics at another point. In some cases short pulses are employed, and in other cases CW or quasi CW transmissions are employed. The latter approach is more suited to obtaining the envelope of a narrowband signal.

An experiment employing both types of signals was conducted in water with an average depth of 4 km.[12] Sources and receivers were suspended at a depth of about 1 km below the tending ships. The major paths were refracted only; the upper path being convex, and the lower one being concave. In the partially saturated regime containing the upper path the amplitude of the signal received from a quasi CW transmission was expected to have a Rayleigh distribution (or an exponential distribution of intensity). The experimental data were consistent with that expectation. In the unsaturated regime containing the lower path, the amplitude was expected to have a log-normal probability density function

$$f(a) = (2/\ va)^{1/2} \exp\ [-2(\ln a + v/4)^2] \qquad (4.27)$$

where v is a parameter depending on the frequency of the transmitted signal. In the frequency region from 1.76 to 2.74 kHz, the parameter is given by

$$v = .35\ f \qquad (4.28)$$

where f is the frequency in kHz.

The correlation function of the intensity of the received signal is predicted to be [13]

$$\langle I(\Delta t)I(0)\rangle = 1 + |Q(\Delta t/t_o)|^2 \qquad (4.29)$$

where the average intensity is $\langle I\rangle = 1$.

Q( ) is the micropath bandwidth function. Figure 4.4 shows the predicted correlation function (heavy solid line) and measured results obtained for reciprocal paths (dashed and solid light lines). For the upper path, the prediction and the measured results are consistent, and the decay time is about 5 minutes. For the lower path, a highly stable reception is predicted which is not consistent with the measurements. The decay time of the latter is about 20 min.

Measurements spanning a period of about a half year were conducted using a projector operating at 368 Hz at a depth of 527 m off Eleuthera and a pair of receivers 1318 km away off Bermuda at depths of 1683 m and 1723 m.[14] Average water depth between the locations was about 4500 m. No firm conclusion was reached regarding the probability density function for the amplitude envelope. The coefficient of variation (σ_A/m_A) for the amplitude envelope for both receivers averaged 0.51; for an amplitude envelope with a Rayleigh distribution, this ratio equals 0.523, and the coefficient of variation for the intensity (σ_I/m_I) equals one. Figure 4.5 shows the normalized autocovariance function for amplitude fluctuations for one of the receivers derived from a sixty-six hour sample. The autocovariance for the intensity envelope is the square of that for the amplitude envelope. For the former, the 1/e decay time is about two minutes.

The statistics of long-range propagation were obtained by having sources of frequencies of 10, 110, and 262 Hz at depths of 110, 23, and 25 m respectively.[15] Signals were recorded from both bottom-mounted and suspended receivers.

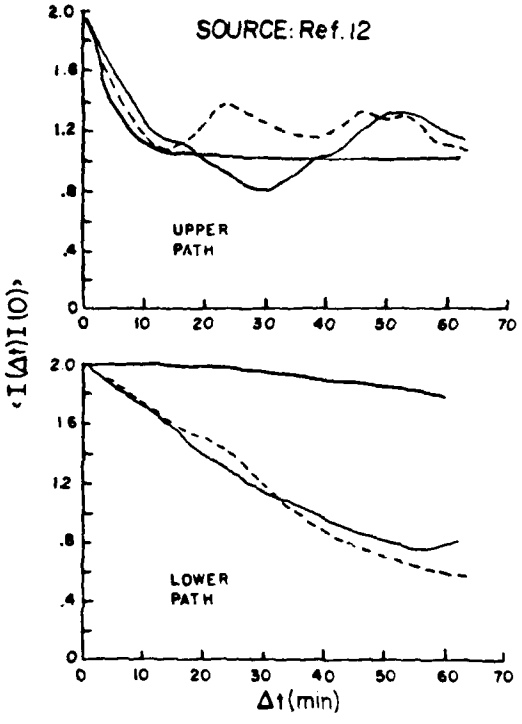

FIGURE 4.4 Intensity correlation for the upper (top figure) and lower (bottom figure) paths at 2250 Hz.

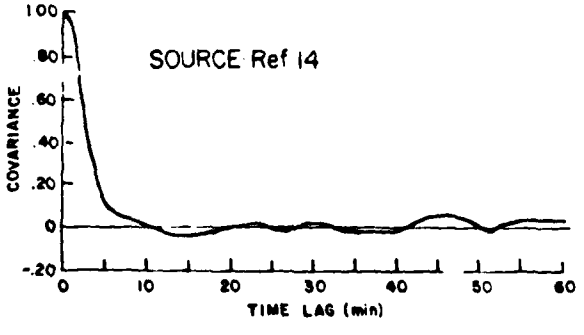

FIGURE 4.5 Normalized autocovariance function for amplitude fluctuations.

Only segments with a mean range greater than 600 km and a mean range rate greater than 10 km/hr were used. Estimates of σ_I/m_I of .89, 1.18, and 1.14 were obtained for the frequencies 10, 110, and 262 Hz respectively. These ratios are reasonably consistent with a Rayleigh distribution for the amplitude envelope and an exponential distribution for the intensity envelope, as predicted for long ranges and a range spread encompassing at least one convergence zone. However, neither the exponential distribution or any of several other candidate distributions produced a good fit to the data at all three frequencies.

Correlation times were calculated by dividing the duration of a data segment by the number of independent samples reported in [15]. Values obtained are 18.3, 4.5, and 1.9 min. for frequencies of 10, 110, and 262 Hz respectively. These apply to range rates greater than 10 km/hr. A correlation time of 2 min. was reported for propagation at 368 Hz from a fixed projector to fixed receivers.[14]

From this limited base of data it can be concluded that relaxation times of both signals and noise can range from much shorter to much longer than a typical post-rectification averaging time, depending on the circumstances.

5.0 FALSE ALARM PROBABILITY - COMMON NOISE POWER ENVELOPE

A single channel (with threshold formation) of the multi-channel analog is shown in Figure 2.1, and an equivalent form is shown in Figure 2.2. If the noise inputs have a common power envelope, then the ith sample of the output of the summer can be represented by

$$Y_i = P_i \left[G_{0i}^2 - \frac{c}{2} \left(G_{-1i}^2 + G_{1i}^2\right)\right] \tag{5.1}$$

$$= P_i\left(J_i - \frac{c}{2} K_i\right) \tag{5.2}$$

where J_i is a chi-squared variate with one degree of freedom,

K_i is a chi-square variate with two degrees of freedom, independent of J_k, all k.

The test statistic is then

$$Z = \sum_{i=1}^{n} P_i\left(J_i - \frac{c}{2} K_i\right) \tag{5.3}$$

where n is the number of independent samples.

When the number of independent samples is large, then the test statistic Z is Gaussian given $\{P_i\} \equiv \underline{P}$, and the approach discussed in the Appendix of [1] can be employed to obtain results for the limiting cases of fast and slow envelope fluctuations. This approach requires the mean and variance of the test statistic given $\underline{P}$. These can be readily derived

using the recursion formula for chi-square variates:

$$m_{n+1} = (d + 2n)m_n, \tag{5.4}$$

where d is the number of degrees of freedom.

The conditional mean of (5.3) is then

$$E(Z|\underline{P}) = (1-c) \sum_{i=1}^{n} P_i \tag{5.5}$$

Squaring (5.3) gives

$$Z^2 = \sum_i \sum_j (J_i J_j - c K_i J_i + \frac{c^4}{4} K_i K_j) , \tag{5.6}$$

and taking the conditional expected value gives

$$E(Z^2|\underline{P}) = \sum_i P_i^2 (3 - 2c + 2c^2) + \sum_{i} \sum_{j \neq i} P_i P_j (1 - 2c + c^2) \tag{5.7}$$

$$= \sum_i P_i^2 (2 + c^2) + \sum_i \sum_j P_i P_j (1 - 2c + c^2) \tag{5.8}$$

The second term is seen to be the square of the conditional mean as given by (5.5); thus the conditional variance is

$$\text{Var}(Z|\underline{P}) = (2 + c^2) \sum_{i=1}^{n} P_i^2 \tag{5.9}$$

The conditional mean and variance can be expressed more compactly as

$$E(Z|\underline{P}) = (1 - c)A \tag{5.10}$$

$$Var(Z|\underline{P}) = (2 + c^2)B \tag{5.11}$$

where $A = \sum_i P_i$

$B = \sum_i P_i^2$

Then (A-10) of [1] can be expressed as

$$P_F = \int_0^\infty da \int_0^\infty db \quad f_{AB}(a,b) P\left[\frac{(1-c)a}{\sqrt{(2+c^2)b}}\right] \tag{5.12}$$

Now let $F = A/\sqrt{B} = \dfrac{\sum_i P_i}{\sqrt{\sum_i P_i^2}}$; (5.13)

then $$P_F = \int_0^\infty df\ f_F(f)\ P\left[\frac{1-c}{\sqrt{2+c^2}}\ f\right] \tag{5.14}$$

where P( ) is the normal distribution function.

The two limiting cases can be readily examined. The first is the limiting case of very slow fluctuations with $P_i = p$, all i. Substitution in (5.13) yields

$$F = \frac{np}{\sqrt{np^2}} = \sqrt{n} \tag{5.15}$$

In this case, the density function for F is a delta function at $F = \sqrt{n}$; evaluation of (5.14) yields

$$P_F = P\left(\frac{1-c}{\sqrt{2+c^2}}\sqrt{n}\right) = Q\left(\frac{c-1}{\sqrt{2+c^2}}\sqrt{n}\right) \qquad (5.16)$$

where $Q(\ ) = 1 - P(\ ) = P(-)$. Since the power envelope is constant, the limiting case also represents one with Gaussian noise.

The second is the limiting case of very fast fluctuations. For this case $\sum P_i^2 \simeq nm_p^2$,

$$\sum P_i^2 \simeq nm_{2P} = n(m_p^2 + \sigma_p^2);$$

then

$$F \to \frac{m_p}{\sqrt{m_{2P}}}\sqrt{n} = \frac{\sqrt{n}}{\sqrt{1+(\sigma_p/m_p)^2}} \qquad (5.17)$$

where σ_p/m_p is the coefficient of variation of P_i.

In this case the density of F approaches a delta function located as indicated by (5.17). Evaluating (5.14) gives

$$P_F = Q\left[\frac{(c-1)\sqrt{n}}{\sqrt{(2+c^2)(1+\sigma_p^2/m_p^2)}}\right] \qquad (5.18)$$

If the power envelope is a chi-squared process then (5.17) can be evaluated by (5.4):

$$F \to \frac{d}{\sqrt{(d+2)d}} = \frac{1}{\sqrt{1+2/d}}$$

and

$$P_F = Q\left[\frac{(c-1)\sqrt{n}}{\sqrt{(2+c^2)(1+2/d)}}\right] \qquad (5.19)$$

Table 5.1 shows values of P_F for various values of the threshold parameter c and the number of degrees of freedom d of the chi-squared envelope. The number of averaged independent samples is 10,000, and the envelope fluctuations are very fast. At low threshold settings, the variations of P_F with the degree of fluctuation is less drastic than at high threshold settings. The row labelled " " applies to both Gaussian inputs, and very slow fluctuations as well. As expected, the false alarm probability increases with the degree of envelope fluctuation, which varies inversely with the number of degrees of freedom.

TABLE 5.1

False Alarm Probability - Fast Fluctuations

	threshold value c		
d	1.05	1.07	1.09
2	2.2 E-2	2.6 E-3	1.8 E-4
4	1.0 E-2	6.3 E-4	1.9 E-5
8	5.6 E-3	2.1 E-4	3.3 E-6
∞	2.3 E-3	3.9 E-5	2.3 E-7

For estimating P_F by simulation, the analog for a channel with a threshold formed from two neighboring channels can be simplified to the form shown in Figure 5.1. The input labelled E_i represents two independent squared normal inputs of the two threshold channels. The input labelled G_i represents the normal input to the center channel.

Table 5.2 shows values of false alarm probabilities for various threshold values c, and various noise power envelope relaxation times. The number of terms in the post-rectification sum is 60, and the noise power envelope is a chi-squared process with four degrees of freedom. For the limiting case of very slow fluctuations, the values were calculated by the method developed in Section 3.0. The values in the next two rows were obtained by simulation using the scheme depicted in Figure 5.1. The number of output samples was 10,000 in order to achieve acceptable accuracy. Results for the very fast envelope fluctuations were calculated by means of (5.19). In all columns it is seen that the false alarm probability varies inversely with the relaxation time of the noise power envelope. Also note that the variation of the false alarm values with relaxation time is greater for larger values of the threshold value c. For example, the ratio of P_F for fast fluctuations to that for slow fluctuations is 2.5 for c = 1.6, whereas the ratio for c = 2.2 is about 19. It is the latter case that is more relevant to sonar operation.

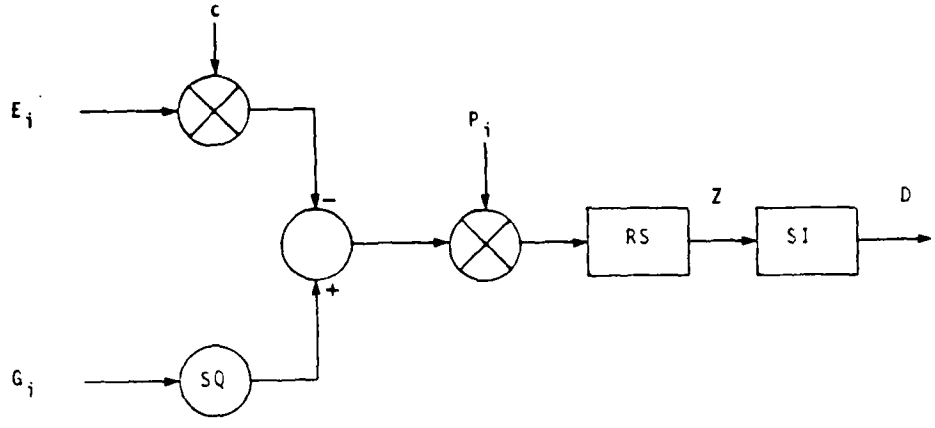

E_i exponential variate, mean 1

G_i normal variat, mean 1, unit variance

c threshold factor

P_i chi-squared envelope variate

RS running sum

Z test statistic

SI set indicator

D detection decision

FIGURE 5.1 Simulation Analog for False Alarms

TABLE 5.2

False Alarm Probabilities - Various Cases

	threshold value c			
envelope	1.6	1.8	2.0	2.2
slow	.0151	.0033	.0007	.0001
m_N = 60	.0258	.0072	.0019	.0003
m_N = 20	.0326	.0115	.0041	.0014
fast	.0378	.0135	.0049	.0019

m_N is the number of samples in the envelope formation running average.

Section 4.2 discussed beam noise measurements obtained with a 720-element planar array. It was estimated that the relaxation time of the beam noise power envelope was about 13 seconds. Relative to a post-rectification averaging time of two minutes or 120 seconds, the relaxation time is indicative of a fast fluctuation. Thus, the false alarm probability might be at least 10 times as high as that predicted assuming either very slow envelope fluctuations or Gaussian noise.

6.0 DETECTION PROBABILITY — Common Noise Power Envelope

This section concerns the detection of signals with fluctuating power envelopes in a background of noise inputs with a common power envelope. The schematic of the simulation for this case is shown in Fig. 6.1. The schematic for the generation of a power envelope is shown in Fig. 2.4, where, for this case, the lowpass filters LPF are running averagers RA.

Results give the probability of detection as a function of average signal-to-noise power in decibels. Results are compared to that of the special case of Gaussian signals and noise.

6.1 Gaussian Signals and Noise

To provide a check for the case of Gaussian signals and noise, an analytical approximation will be derived, based on the assumption that the test statistic is nearly Gaussian. In that case, (2.13) of Ref. 1 becomes

$$P_D \approx \int_{-C_{ZS}^{-1}}^{\infty} dx\, Z(x) = Q(-C_{ZS}^{-1}) \qquad (6.1)$$

where C_{ZS} is the coefficient of variation of the test statistic when the signal is present

$Z(\ )$ is the Gaussian (0, 1) density function

The inverse of C_{ZS} is given by (6.5) of Ref. 1; for the sampled data case, replace the bandwidth-time product WT by n/2, where n

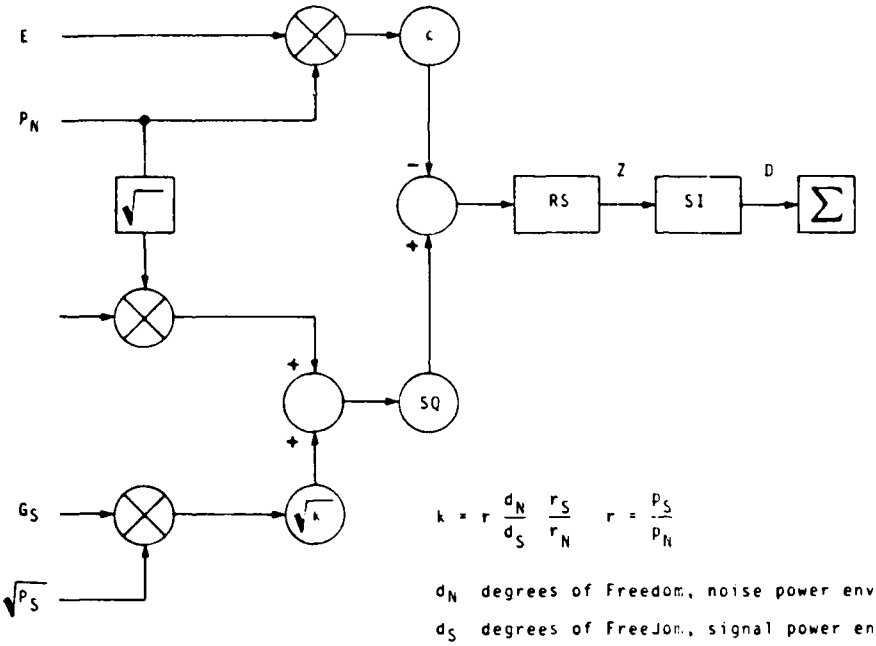

$$k = r \frac{d_N}{d_S} \frac{r_S}{r_N} \qquad r = \frac{P_S}{P_N}$$

d_N degrees of Freedom, noise power envelope

d_S degrees of Freedom, signal power envelope

r_S samples in running average - signal envelope

r_N samples in running average - noise envelope

FIGURE 6.1 Detection Simulation - Common Noise Power Envelope

is the number of independent samples added by the post-rectification running summer. And for a two-channel threshold, let $c_i = c/2$; then (6.5) of Ref. 1 becomes

$$\frac{1}{C_{ZS}} = \sqrt{\frac{n}{2}} \frac{r + 1 - c}{\sqrt{(r + 1)^2 + c^2/2}} \tag{6.2}$$

where $r = p_s/p_n$ is the signal-to-noise power ratio. Substituting (6.2) in (6.1) gives

$$P_D = Q\left[\frac{\sqrt{n/2}\,(c - 1 - r)}{\sqrt{2(r + 1)^2 + c^2/2}}\right] \tag{6.3}$$

Fig. 6.2 shows the transition curve for n = 60 calculated from (6.3). The detection differential (10 $\log_{10}$ r for $P_D = 0.5$) is .8 dB, and the spread (dB between $P_D = 0.2$ and $P_D = 0.8$) is 3.05 dB. For a single-channel analog with a "linear" detector, a deterministic threshold, and a sine wave signal in stationary Gaussian noise [16], the detection differential is -2.7 dB, and the spread is 2.4 dB for n = 64. For the same type of detector and inputs, the detection differential is -13.7 dB and the spread is 2.05 dB for n = 8192.

It is clear from the horizontal axis of Fig. 6.2 that the small-signal regime does not obtain for n = 60, with the consequence that the transition curves that follow cannot be extrapolated to larger values of n. The simulation analog was run with Gaussian signals and noise for n = 60, and the number of output samples was 1000. The results P_S of the simulation are compared with

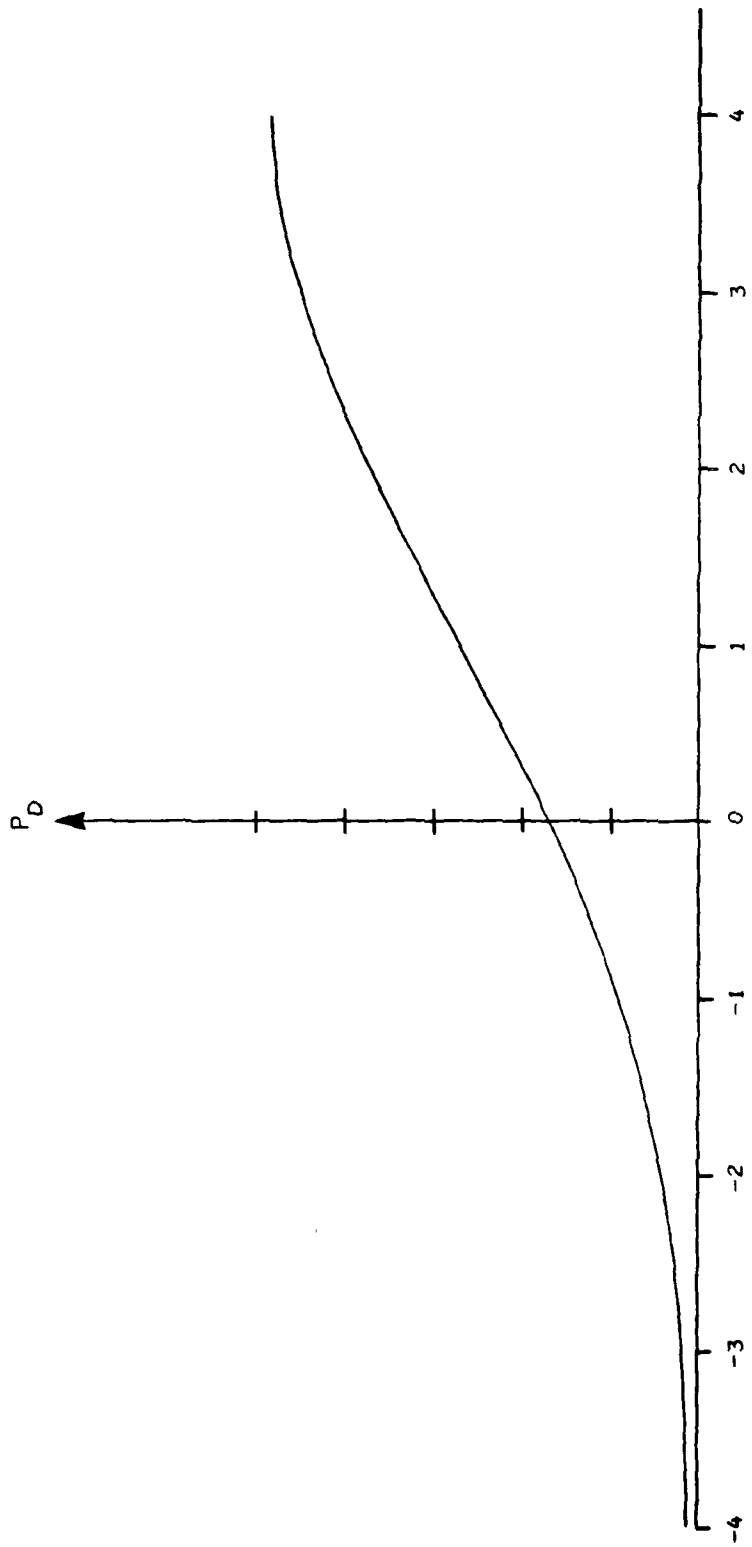

FIGURE 6.2 Transition Curve for n = 60

the results P_A obtained using the approximation (6.3). The differences are seen to be small, and the consistent sign of the differences indicates a bias in the approximations calculated from (6.3).

Table 6.1

Comparison of Simulation and Calculation

10 log r, dB	P_S	P_A	$P_S - P_A$
-3	.039	.038	+.001
-2	.089	.083	+.006
-1	.188	.175	+.013
0	.346	.333	+.013
1	.558	.547	+.011
2	.776	.758	+.018
3	.916	.902	+.014
4	.980	.969	+.011

6.2 Limiting Case — Very Fast Fluctuations

This section derives an analytical result for P_D for the limiting case of signals and noise with fast-fluctuating power envelopes. The procedure followed is the same as that employed in Section 5.0 to obtain P_F. The procedure requires the mean and variance conditioned on random variates derived from the power envelopes. The conditional means and variances will be derived for the continuous input case and then converted to the sampled data case.

Equation (A-3) of Ref. 1 gives the conditional mean for a general case with continuous inputs. For the case of a common

noise power envelope and a two-channel threshold with weighting factor $c_i = c/2$, the conditional mean is

$$E[Z|\underline{P(t)}] = A_S + (1 - c)A_N \tag{6.4}$$

where $\underline{P}(t)$ is the set of power envelopes

$$A_S = T^{-1}\int_0^T du\ P_S(u)$$

T is post-rectification averaging time

$$A_N = T^{-1}\int_0^T du\ P_N(u)$$

Equation (A-9) of Ref. 1 gives the conditional variance for a general case with continuous inputs. For the specific case described above, the conditional variance is

$$\text{Var}\ [Z|P(t)] = (WT)^{-1}\ [B_S + 2B_C + (1 + c^2/2)B_N] \tag{6.5}$$

where W is the input bandwidth

$$B_S = T^{-1}\int_0^T du\ P_S^2(u)$$

$$B_C = T^{-1}\int_0^T du\ P_S(u)P_N(u)$$

$$B_N = T^{-1}\int_0^T du\ P_N^2(u)$$

For the case of fast fluctuations, examination shows that $A_S \rightarrow p_S$, $B_S \rightarrow p_S^2 + \sigma_S^2$, etc.; and if the WT product is sufficient, the distribution approaches normal. For the continuous input case, the detection probability is approximately

$$P_D = Q\left[\frac{\sqrt{WT}[(c - 1)\, p_N - p_S]}{p_S^2 + \sigma_S^2 + 2p_S p_N + (p_N^2 + \sigma_N^2)\,(1 + c^2/2)}\right] \qquad (6.6)$$

For the sampled-data case, the number of independent samples that are averaged is $n = 2WT$; thus

$$P_D = Q\left[\frac{\sqrt{\frac{n}{2}}\,(c - 1 - r)}{\sqrt{r^2\,(1 + C_S^2) + 2r + (1 + C_N^2)\,(1 + c^2/2)}}\right] \qquad (6.7)$$

where $r = p_S/p_N$

$C_S = \sigma_S/p_S$

$C_N = \sigma_N/p_N$

Finally, if the envelopes are chi-squared processes then $C_S^2 = 2/d_S$, $C_N^2 = 2/d_N$, and

$$P_D = Q\left[\frac{\sqrt{\frac{n}{2}}\,(c - 1 - r)}{\sqrt{r^2\,(1 + 2/d_S) + 2r + (1 + 2/d_N)\,(1 + c^2/2)}}\right] \qquad (6.8)$$

Comparison of (6.7) with (6.3) for the Gaussian input case shows that the denominator of the argument is larger; hence, the transition curve for the fast fluctuation case will have a larger spread in signal-to-noise power ratio.

6.3 Limiting Case — Very Slow Fluctuations

This section derives an analytical result for P_D for the limiting case of signals and noise with signal and noise power envelopes that are very slowly fluctuating. In the limit, the power envelopes are random variates vice random processes. For this case, the general result is*

$$P_D = \int_0^\infty dr\ f_R(r)\ g(r) \tag{6.9}$$

where $f_R(\ )$ is the density of R

$R = p_S/p_N$

$g(\ )$ is the transition curve for Gaussian inputs.

If the envelope variates are gamma-distributed, then the probability density of R is given by (6.27) of Ref. 1. For the particular case of chi-squared variates, then the probability density is

$$f_R(r) = \frac{\Gamma\left(\frac{d_S}{2} + \frac{d_N}{2}\right)}{\Gamma\left(\frac{d_S}{2}\right)\Gamma\left(\frac{d_N}{2}\right)} \left(\frac{d_S}{\bar{r}d_N}\right) \frac{r^{\frac{d_S}{2} - 1}}{\left(1 + \frac{d_S}{d_N} \cdot \frac{r}{\bar{r}}\right)^{\frac{d_S + d_N}{2}}} \tag{6.10}$$

where $\bar{r} = p_S/p_N$

*See (1.2) of Ref. 1.

Given an adequate time-bandwidth product, then the transition curve for Gaussian inputs is given by (6.3). Thus, for the limiting case of very slowly fluctuating chi-squared power envelopes, the probability of detection is found by substituting (6.3) and (6.10) in (6.9).

6.4 Transition Curves

Transition curves obtained by both calculation and simulation are shown in Fig. 6.3. The transition curve for Gaussian inputs, discussed in Section 6.1, shows the least spread in signal-to-noise power ratio. All the other curves pertain to chi-squared envelopes with two degrees of freedom for the signal (appropriate for propagation over a large range), and four degrees of freedom for the noise. These curves clearly show that the faster the fluctuation, the smaller the spread in signal-to-noise power ratio. The curves diverge more at the positive signal-to-noise levels than at the negative. At the positive levels, the signal power dominates, and in this case, it has a greater variability than the noise.

The solid and dashed lines in Fig. 6.4 repeat two of the transition curves shown in Fig. 6.3: $n_S = 20$, $n_N = 20$ and $n_S = 60$, $n_N = 60$. The triangles mark points obtained by simulation for the case $n_S = 20$, $n_N = 60$. For $\bar{R} \geq 1$ dB, these points fall very near to the $n_S = 20$, $n_N = 20$ curve; this is reasonable since both cases have the same signal power envelope relaxation time. For $\bar{R} \leq -1$ dB, these points fall nearer the $n_S = 60$, $n_N = 60$ curve; this is reasonable since these cases have the same noise power envelope relaxation time. The circles mark points obtained by simulation for the case $n_S = 60$, $n_N = 20$. For $\bar{R} \geq 2$ dB, these points fall very close to the curve for the $n_S = 60$, $n_N = 60$ case. For $\bar{R} \leq -2$ dB, these points fall very near the curve for the $n_S = 20$, $n_N = 20$ case.

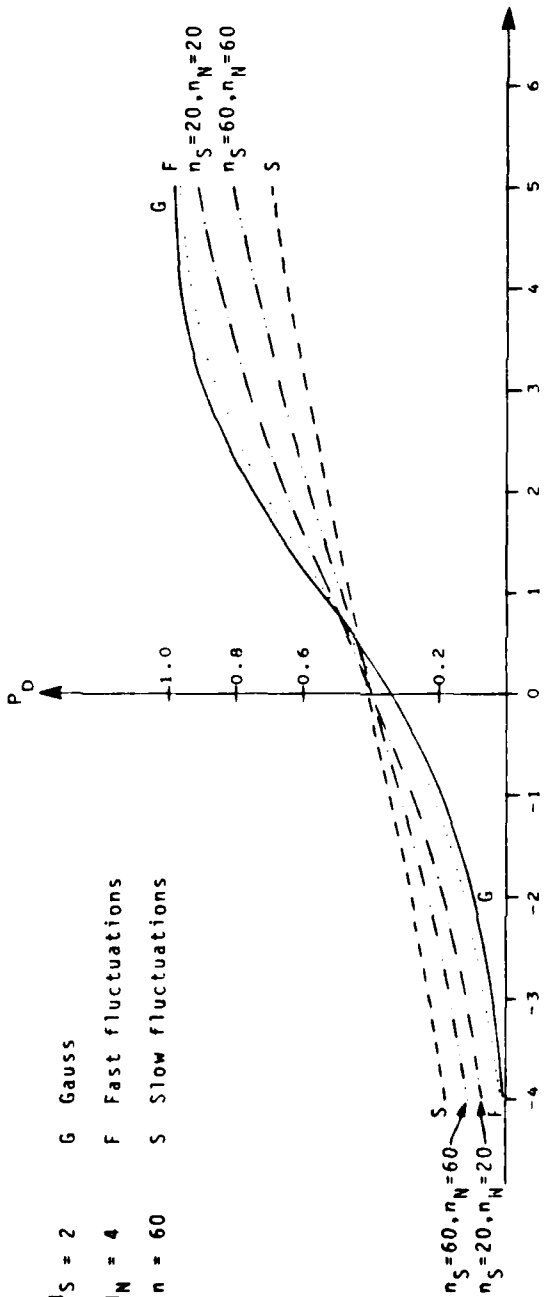

FIGURE 6.3 Transition Curves

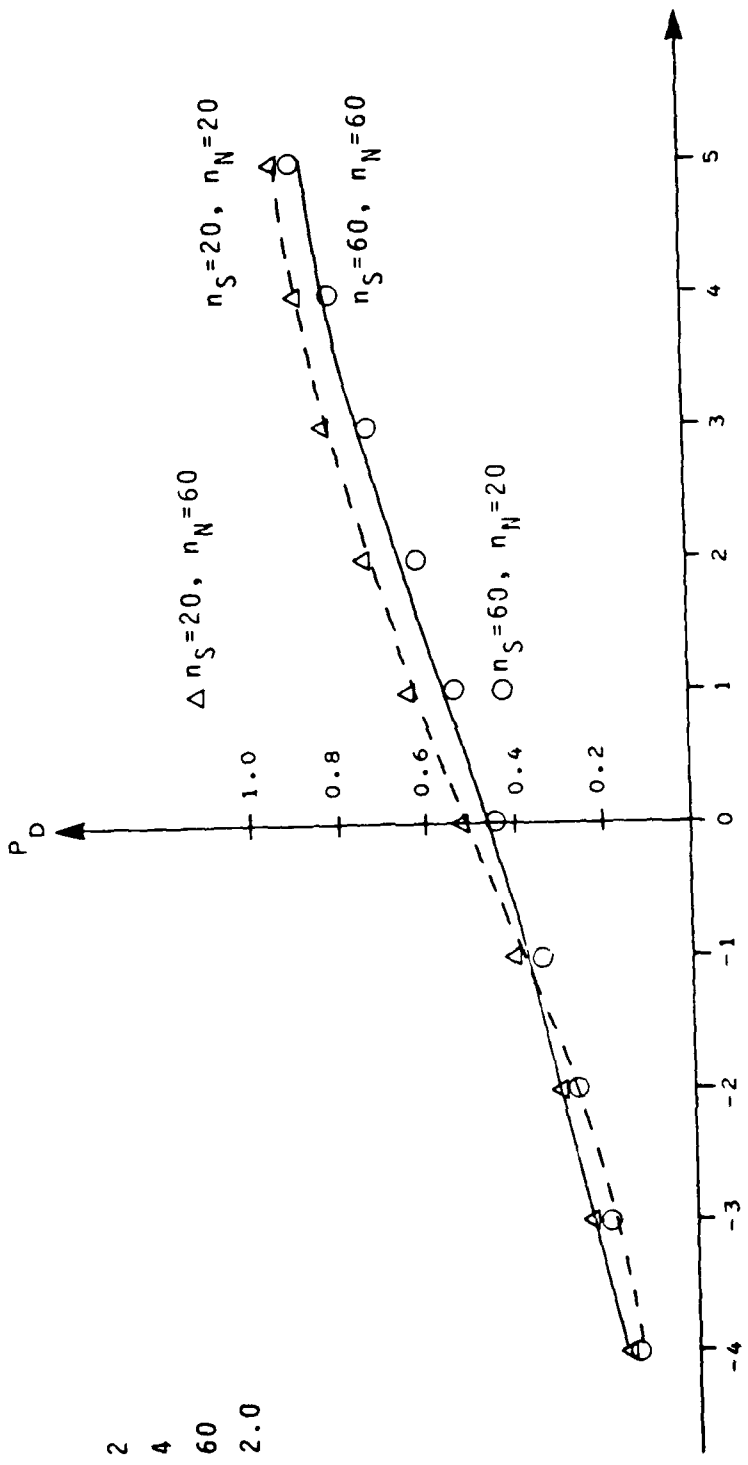

FIGURE 6.4 Transition Curves-Common Noise Power Envelope

Each transition curve can be partially characterized by a pair of numbers: $\bar{R}_T$, the value of $\bar{R}$ for which $P_D = 0.5$; and the spread in dB between $\bar{R}$ values corresponding to $P_D = 0.2$ and $P_D = 0.8$. Threshold and spread values are shown in Table 6.2, which shows that the range of $\bar{R}_T$ is only 0.7 dB, whereas the range of spreads is almost 8 dB.

Historically, predictions of detection performance usually fall into one of two categories. One of them assumes that the inputs are Gaussian, and the other assumes that the relaxation time of the inputs is very large compared to the post-rectification averaging time. These assumptions lead to the extreme transition curves labeled G and S on Fig. 6.3 respectively. The latter assumption could lead to excessive optimism regarding the detection of sources at long ranges from multiple independent observations. The former assumption could lead to excessive optimism regarding detection performance at short ranges.

Table 6.2

Threshold and Spread Values — Common Noise Power Envelope

Signal	Noise	$\bar{R}_T$, dB	Spread, dB
Gaussian	Gaussian	0.8	3.1
$d_s = 2$, fast	$d_s = 4$, fast	0.8	3.7
" , $n_S = 20$	" , $n_N = 20$	0.8	5.3
" , $n_S = 20$	" , $n_N = 60$	0.6	5.8
" , $n_S = 60$	" , $n_N = 20$	1.3	6.3
" , $n_S = 60$	" , $n_S = 60$	1.1	7.2
" , slow	" , slow	1.5	11.0

7.0 PARTIALLY-CORRELATED NOISE POWER ENVELOPES

7.1 Introduction

The previous section dealt with a case in which a noise power envelope was common to the inputs of all of the channels. This is equivalent to saying that the noise power envelopes are fully correlated. This section deals with a case in which the noise power envelopes are partially correlated. Ref. 11 presents data showing the correlation of averaged power levels of beam outputs derived from a line array operating in a frequency band in which the dominant noise is generated by ships. The data are not repeated here because of their security classification.

Figure 7.1 illustrates a means for generating three partially-correlated chi-squared envelopes with four degrees of freedom. The correlation between the center channel envelope and that of a threshold channel is 0.75, and the correlation between the threshold channels is 0.5. For greater generality, the running averagers (RA) could be replaced by linear lowpass filters.

Figure 7.2 illustrates the flow diagram for the multichannel analog and its input components appropriate for obtaining transition curve data. False alarm probabilities can also be estimated by setting the parameter k equal to zero.

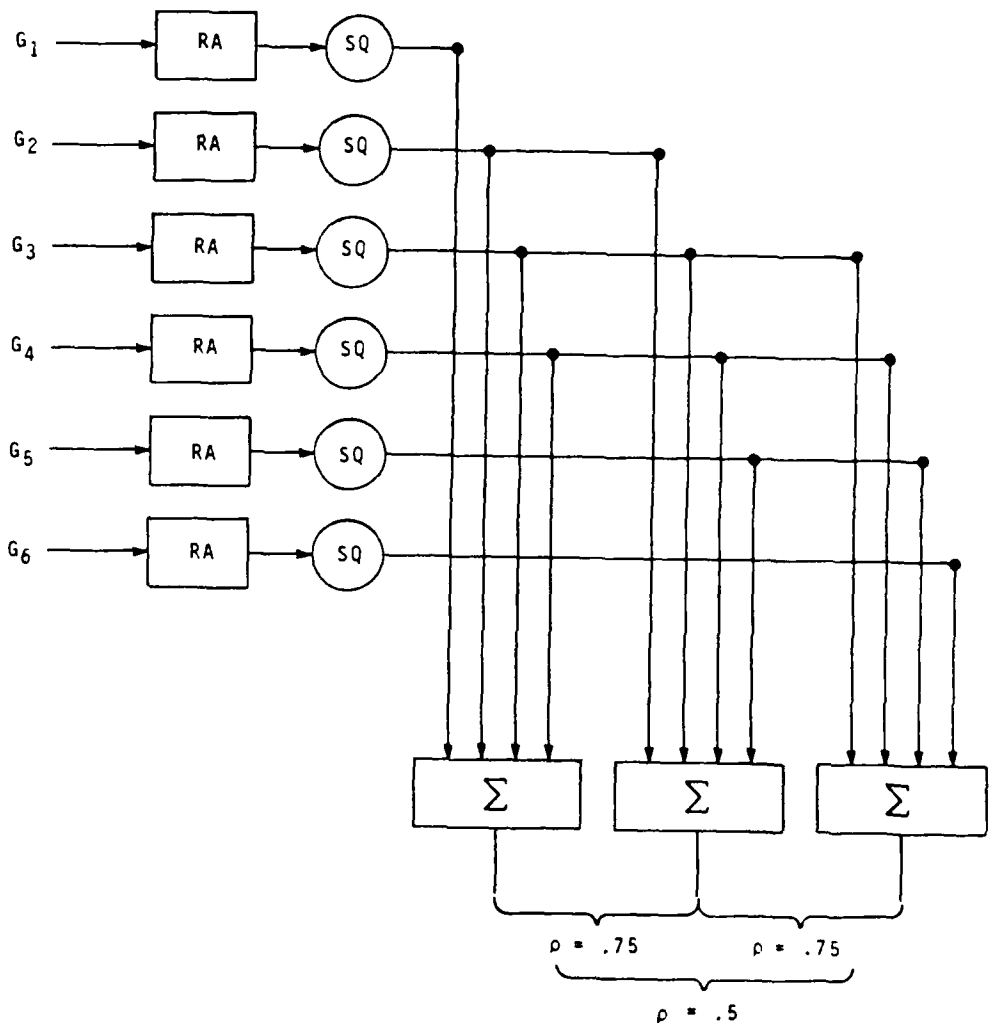

FIGURE 7.1 Synthesis of Partially-Correlated Noise Power Envelopes.

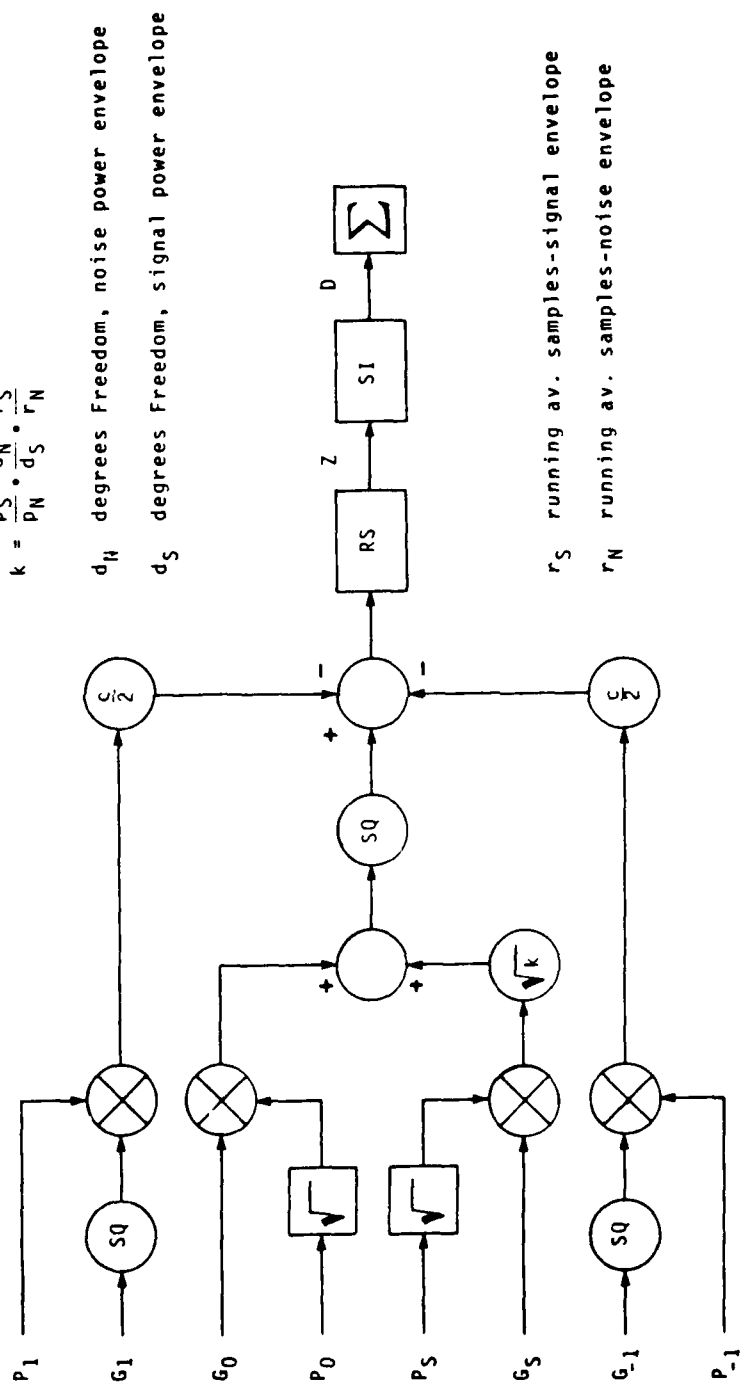

FIGURE 7.2 Detection Simulation-Partially-Correlated Noise Power Envelope

7.2 Limiting Case-Very Slow Fluctuations

The limiting case of very slow fluctuations will be examined first with the objective of predicting false alarm probability. In this case, the power envelopes are random variates rather than random processes. A single channel (with threshold formation) of the multichannel analog is shown in Figure 2.1, and an equivalent form is shown in Figure 2.2. With power envelopes described above, the test statistic can be expressed as

$$Z = \sum_{i=1}^{n} [P_0 G_{0i}^2 - \frac{c}{2} (P_1 G_{1i}^2 + P_{-1} G_{-1i}^2)] \quad (7.1)$$

$$= P_0 \sum_{i=1}^{n} G_{0i}^2 - \frac{c}{2} (P_1 \sum_{i=1}^{n} G_{1i}^2 + P_{-1} \sum_{i=1}^{n} G_{-1i}^2) \quad (7.2)$$

where the subscript 0 denotes the center channel. The sums shown in (7.2) represent chi-square variates of n degrees of freedom. As n increases, the distribution of the chi-squared variate approaches normal. If the sums are assumed normal, then

$$Z = P_0 G_0 - \frac{c}{2} (P_1 G_1 + P_{-1} G_{-1}) \quad (7.3)$$

where G_i is a Gaussian random variate with mean n and variance $2n$, $i = -1, 0, 1$

If the envelopes P_i are syntehsized in a manner analogous to Figure 7.1 then

$$Z = G_0 \sum_{i=2}^{5} K_i - \frac{c}{2} (G_1 \sum_{i=1}^{4} + G_{-1} \sum_{i=3}^{6}) \quad (7.4)$$

where $K_i = G_{Ei}^2$

G_{Ei} = Gauss (0,1)

Finally, $P_F = P(Z > 0)$ (7.5)

Equation (7.4) and (7.5) form the basis for estimating P_F by means of a Monte Carlo simulation.

Figure 7.3 shows the false alarm probability for a single observation as a function of the threshold parameter c for both partially- and fully-correlated slowly-fluctuating noise power envelopes. The difference of the false alarm probabilities is seen to increase with threshold value. At c = 2.2, the partially correlated noise power envelope yields a false probability that is almost 100 times that produced by the fully correlated envelope.

7.3 Limiting Case - Very Fast Fluctuations

A means will be derived for calculating the false alarm probability for the case of partially-correlated noise power envelopes with very fast fluctuations. The approach discussed in the Appendix of [1] will be employed. For the work at hand, (A-10) of [1] can be written as

$$P_F = \int_0^\infty dr\ f_R(r)\, P(r) \qquad (7.6)$$

where P() is the distribution function for a normal (0,1) variate,

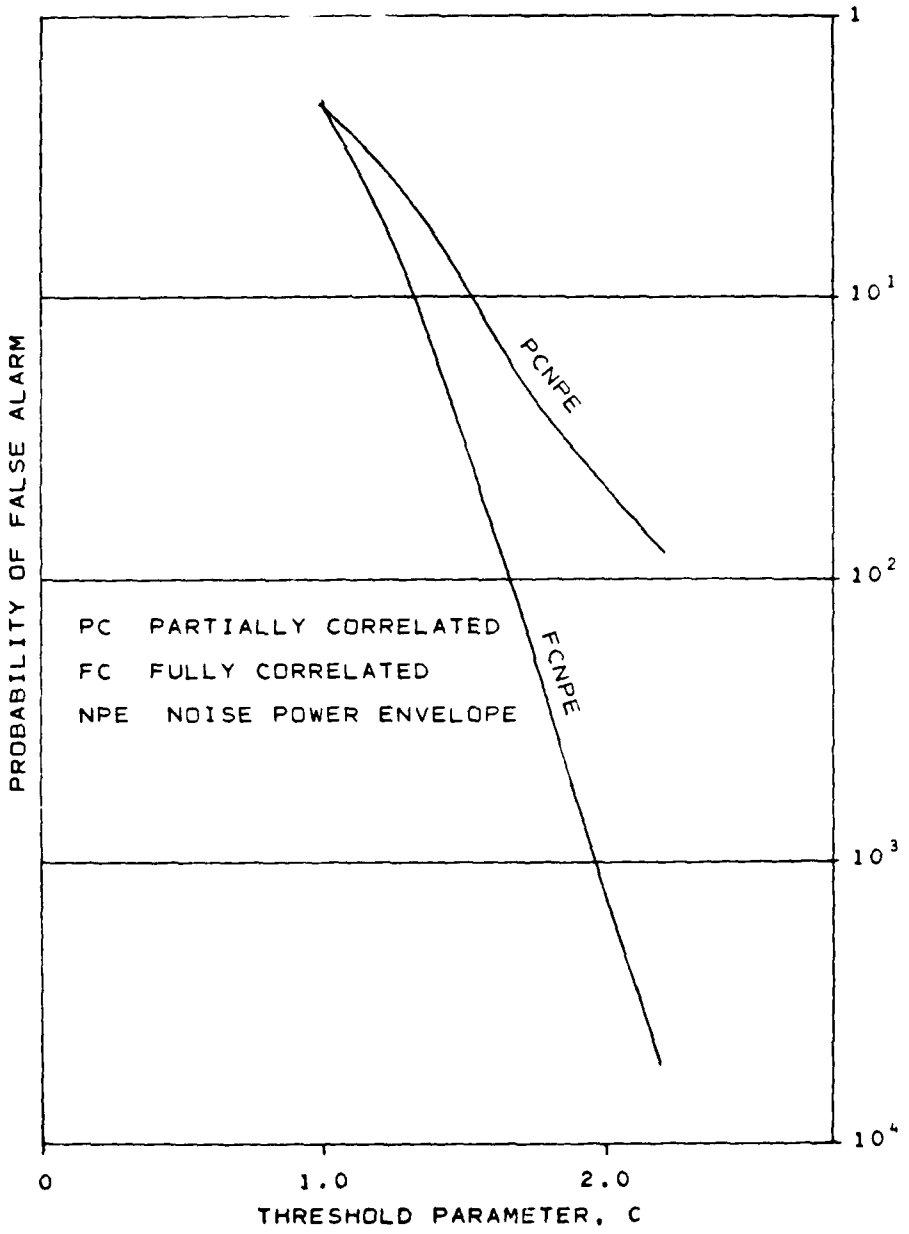

FIGURE 7.3 Effect of Correlation of Noise Power Envelope -- Very Slow Fluctuations

$f_R()$ is the probability density function for R,

$$R = \frac{E(Z|\underline{P})}{\sqrt{V(Z|\underline{P})}} \tag{7.7}$$

V() denotes the variance of the argument

$\underline{P} = \{P_{ij}\}$ denotes a set of sample values of the noise power envelopes.

For this case, the test statistic can be expressed as

$$Z = \sum_{i=1}^{n} [P_{0i}G_{0i}^2 - \frac{c}{2}(P_{1i}G_{1i}^2 + P_{-1i}G_{-1i}^2)] \tag{7.8}$$

The expected value of the test statistic Z given the values denoted by $\underline{P}$ is

$$E(Z\ \underline{P}) = \sum_{i=1}^{n} [P_{0i} - \frac{c}{2}(P_{1i} + P_{-1i})] \tag{7.9}$$

If the envelopes are synthesized according to the scheme depicted by Figure 7.1, and if only one term is employed in the running averagers (this corresponds to the most rapid fluctuation), then the jth sample of the power envelope for channel i can be expressed as

$$P_{ij} = \sum_{k=i+2}^{i+5} H_{kj}^2 \tag{7.10}$$

where H_{kj} is the jth sample of input k, a normal random variate (0,1), statistically independent of H_{pq} unless $k = p$ and $j = q$.

Substituting (7.10) in (7.9) and collecting terms gives

$$E(Z|\underline{P}) = \sum_{i=1}^{n} [-\tfrac{c}{2} H_{1i}^2 + (1-\tfrac{c}{2})H_{2i}^2 + (1-c)H_{3i}^2 + (1-c)H_{4i}^2 + (1-\tfrac{c}{2})H_{5i}^2 - \tfrac{c}{2}H_{6i}^2] \quad (7.11)$$

If n is large, then

$$\sum_{i=1}^{n} H_{ij}^2 \approx n, \; j = 1,2,3,4,5,6$$

and $$E(Z|\underline{P}) \approx 4n(1-c) \quad (7.12)$$

The conditional variance of the test statistic is found by obtaining the conditional mean square and subtracting the square of the conditional mean. The result obtained is

$$V(Z|\underline{P}) = 2 \sum_{i=1}^{n} [P_{0i}^2 + \tfrac{c^2}{4} (P_{1i}^2 + P_{-1i}^2)] \quad (7.13)$$

Squaring and summing over n samples gives

$$\sum_{j-1}^{n} P_{ij} = \sum_{k=i+2}^{i+5} \sum_{\ell=i+2}^{i+5} \sum_{j=1}^{n} H_{kj}^2 H_{\ell j}^2 \quad (7.14)$$

If n is large, then

$$\sum_{j=1}^{n} P_{ij} \approx n\left[\sum_{\substack{k=i+2 \\ k\neq\ell}}^{i+5} \sum_{\ell=i+2}^{i+5} 1 + \sum_{k=i+2}^{i+5} 3\right] \quad (7.15)$$

$$= n\left[\sum_{k=i+2}^{i+5} \sum_{\ell=i+2}^{i+5} 1 + \sum_{k=i+2}^{i+5} 2\right] \quad (7.16)$$

$$= 24n$$

Applying this result in (7.12) gives

$$V(Z|P) = 24n(2 + c^2) \tag{7.18}$$

Substituting (7.12) and (7.18) in (7.7) and simplifying gives

$$R = \frac{\sqrt{n}(1-c)}{\sqrt{(2+c^2)3/2}} \tag{7.19}$$

The density function for R is approximately a delta function at the location indicated by (7.19). Evaluation of (7.6) yields

$$P_F = Q\left[\frac{\sqrt{n}(1-c)}{\sqrt{(2+c^2)3/2}}\right] \tag{7.20}$$

The result is identical to (5.19) with $d_N = 4$. That is, for fast fluctuations, the false alarm probability is independent of the degree of envelope correlation.

7.4 False Alarm Probability

Table 7.1 shows values of flase alarm probabilities for various threshold values c, and various noise power envelope relaxation times. The number of terms in the post-rectification sum is 60, and each noise power envelope is a chi-squared process with four degrees of freedom. For the limiting case of very slow fluctuations, the values were generated by the Monte Carlo method described in Section (7.2). The values in the next two rows are obtained by simulation as described in

TABLE 7.1

False Alarm Probability - Partially Correlated Envelope

	value of c, threshold parameter			
envelope	1.6	1.8	2.0	2.2
slow	.0733	.0365	.0212	.0123
$n_N = 60$	.0674	.0305	.0141	.0063
$m_N = 20$	.0510	.0203	.0078	.0046
fast	.0378	.0135	.0049	.0019

Section 7.1. The number of output samples was 10,000 in order to achieve acceptable accuracy. Results for the very fast envelope fluctuations were calculated by means of (7.20). In all columns it is seen that the false alarm probability varies directly with the relaxation time of the power envelope. This is just the reverse of the case of the fully-correlated noise power envelopes (i.e., the common noise power envelope). Comparison of the last rows of Tables 7.1 and 5.2 show common values of false alarm probabilities for the limiting case of fast fluctuations for the two classes of envelopes. Again, it is noted that the variation of false alarm probability with relaxation time is greater for larger values of the threshold value c. For example, the ratio of P_F for slow fluctuations to that for fast fluctuations is 1.94 for c = 1.6, whereas the ratio for c = 2.2 is about 6.5.

The greatest disparity between the values in Tables 7.1 and 5.2 occurs for the limiting case of very slow fluctuations. Recall also that the first line of Table 5.2 also corresponds to a Gaussian noise input. For a threshold value of 2.2, the false alarm probability for the partially correlated noise power envelope is about 120 times that for a fully-correlated noise power envelope or for Gaussian noise inputs.

7.5 Transition Curves

Four transition curves obtained by simulation are represented in Figure 7.4. All curves pertain to chi-squared envelopes with two degrees of freedom for the signal (appropriate for propagation over a long range), and four degrees of freedom for the noise. The dashed and solid curves pertain to n_S=20, n_N = 20, and n_S = 60, n_N = 60 respectively. Of these, the former shows the least spread. The triangles mark points obtained for the case n_S = 20, n_N = 60. For $\bar{R} \geq 0$ db, these points fall near the n_S = 20, n_N = 20 curve; this is reasonable since both cases have the same signal power envelope relaxation time. For $R \geq -2$ dB, the points in the triangles approach the n_S = 60, n_N = 20 curve; this is expected since these cases have the same noise power envelope relaxation time. Similar remarks can be made about the cases represented by the solid curve and the circled points. In these respects the transition curves for the cases of partially-correlated noise power envelopes are similar to those for the common noise power envelope.

Table 7.2 gives values for $\bar{R}_T$, the value of $\bar{R}$ for which $P_D = 0.5$, and the spread in dB between $\bar{R}$ values corresponding to $P_D = 0.2$ and $P_D = 0.6$.

TABLE 7.2

Threshold and Spread Values-Partially-Correlated Noise Power Envelopes

Signal, d_s=2	Noise, d_s=4	$\bar{R}_T$, dB	spread, dB
20	20	0.0	5.7
20	60	-0.2	6.2
60	20	0.7	6.8
60	60	0.4	7.2

The range of threshold values (maximum minus minimum value) is only 0.6 dB, whereas the range of spread values is 1.5 dB. Comparing the entries in Table 7.2 to the corresponding entries in Table 6.2 will not be highly informative since the values of the threshold parameters were different (2.0 vice 2.2, respectively). Qualitatively, the transition curves for the two cases (partially and fully correlated noise power envelopes) are similar.

REFERENCES

1. M. Moll, "Prediction of Passive Sonar Detection Performance in Environments with Acoustical Fluctuations," Bolt Beranek and Newman Inc. Report No. 3656, Nov. 1978, ADA 062 487.

2. M. Moll, "A Compound Random Process for Underwater Ambient Acoustic Noise," Proceedings of the IEEE International Conference on Acoustics, Speech, and Signal Processing, April 9, 10, 11, 1980, pp 124-129.

3. T. Arase and E.M. Arase, "Deep-Sea Ambient Noise Statistics," J. Acoust. Soc. Am., Vol. 44, No. 6, pp 1679-1684, Dec., 1968.

4. J.B. Farison, "On Calculating Moments for Some Common Probability Laws," IEEE Transactions on Information Theory, Vol. IT-11, No. 4, Oct. 1965, pp 586-589.

5. I.S. Gradshteyn, I. M. Ryzhils, Table of Integrals, Series, and Products, Academics Press, New York, 1965.

6. G. Vezzosi and B. Picinbono, "Detection d'un signal certain dans un bruit spheriquement invariant, structure et caracteriques des receptions," Ann. des Telecommunications, Vol. 27, pp. 95-110, 1972.

7. B. Picinbono, "Spherically Invariant and Compound Gaussian Stochastic Processes," IEEE Trans. on Information Theory, Vol. IT-16, No. 1, pp. 77-79, January 1970.

8. R.F. MacKinnon and M.J. Wilmut, "Minicomputers, Statistics, and Artic Ambient Noise," USNJUA, Vol. 23, No. 4, October 1973, pp. 431-436

9. W.J. Jobst and S.L. Adams, "Statistical Analysis of Ambient Noise," J. Acoust. Soc. Am., Vol. 62, No. 1, pp. 63-71, July 1977.

10. V.C. Anderson,"Nonstationary and nonuniform oceanic background in a high-gain acoustic array," J. Acoust. Soc. Am. Vol. 67, No. 4, April 1980, pp. 1170-1179.

11. R.H. Nichols, H.J. Nichols, C.E.Sayer, "Ambient Noise Correlation Among Array Beams," USNJUA, Vol. 27, No. 4, October 1977, p. 723.

12. P.F. Worcester, "Reciprocal Acoustic Transmission in a Mid-Ocean Environment: Fluctuations," J. Acoust. Soc. Am., Vol. 66, No. 4, p. 1173, October 1979.

13. S.M. Flatté, R. Dashen, W.H. Munk, K.M. Watson, and F.Zachariasen, Sound Transmission Through a Fluctuating Ocean, Cambridge University Press, Cambridge, 1979.

14. G.E. Stanford, "Fluctuations of a CW Signal in the Ocean," J. Acoust. Soc. Am., Vol 55, No. 5, May 1974.

15. G.V. Frisk, "Intensity Statistics for Long-Range Acoustic Propagation in the Ocean," J. Acoust. Soc. Am., Vol. 64, No. 1, pp. 257-259, July 1978.

16. G.H. Robertson, "Operating Characteristics for a Linear Detector of CW Signals in Narrowband Gaussian Noise," The Bell System Technical Journal, April 1967, pp. 755-774.

APPENDIX A

Moments of the Test Statistic and P_F Predictions

An analytical method was devised to calculate the detection performance of the multichannel analog operating with fluctuating inputs. A means was found to approximate the density function of the test statistic by an expansion of the form

$$f_Z(x) = g(x) \sum_{i=1}^{n} a_i x^i \qquad \text{(A-1)}$$

where $g(x)$ is a basis density function. The coefficients a_i of the expansion are determined by requiring that its first n moments match those of the test statistic. The resulting set of n + 1 equation is

$$\sum_{i=0}^{n} a_i m_{k+1} = \alpha_k, \quad k = 0, 1, 2, \ldots, n \qquad \text{(A-2)}$$

where m_i is the $i^{\underline{th}}$ moment of the basis density function

α_k is the $k^{\underline{th}}$ moment of the test statistic

Moments to the third order were previously derived [1] and applied to predict detection performance. More recently, the fourth-order moment was derived, and the moments were applied to predict false alarm probability. Results of those calculations are presented in the sequel, along with the fourth-order moment of the test statistic, shown below.

$$\mu_{4Z} = 12(p_N\beta)^4 \{s^{-2}(I_{DS}^2 + 4s^{-1} I_{QS})\, u^4$$
$$+ s^{-1} I_{DS} [2n^{-1} I_{DN} + (1+2n^{-1})\gamma^{-2}]\, u^2$$
$$+ n^{-2} (I_{DN}^2 + 4n^{-1} I_{QN})$$
$$+ \tfrac{1}{2}\gamma^{-2}n^{-1} [2I_{DN} + 16n^{-1} I_{TN} + 4n^{-1} I_{DN}(1+2I_{DN}) + 16n^{-2}(2I_{TN} + I_{QN})]$$
$$+ \tfrac{1}{4}\gamma^{-4} [1+4n^{-1}(1+2I_{DN}) + 32n^{-2} I_{DN} + 4n^{-2}(1+2I_{DN}^2) + 16n^{-3}(2I_{DN}+I_{QN})\}$$

(A-3)

where p_N is average noise power

$$\beta = \gamma\sqrt{\frac{1+m^{-1}}{WT}}$$

γ is the false alarm parameter. For a normal input, the probability of false alarm is $P(-\gamma) = Q(\gamma)$.

$P(\ )$ is the cumulative distribution for a zero-mean, unit variance normal random variable,

$Q(\ ) = 1 - P(\ )$

m is the number of channels employed for threshold formation,

W is the input bandwidth of the receiver,

T is post-rectification averaging time,

s is the number of degrees of freedom of the signal power envelope.

the subscripts S and N denote signal and noise respectively,

$$I_D = T^{-2}\int du \int dv\; r^2(u-v) \qquad (A-4)$$

$$I_T = T^{-3}\int du \int dv \int dw\; r(u-v)r(v-w)r(w-u) \qquad (A-5)$$

$$I_Q = T^{-4}\int du \int dv \int dw \int dx\ r(u-v)r(v-w)r(w-x)r(x-u) \qquad (A\text{-}6)$$

the limits of integration are from 0 to T.

r() is the autocovariance function for the (Gaussian) components of the chi-squared envelope processes.

m is the autocovariance function for the (Gaussian) components of the chi-squared envelope process.

The integrals defined in the previous paragraph were derived for the case in which

$$r(t) = \exp\left[-|t|(2D)^{-1}\right] \qquad (A\text{-}7)$$

where D is the relaxation time of the power envelope. The results are

$$I_D = 2\frac{D}{T}\left[1 + \frac{D}{T}\left(e^{-T/D} - 1\right)\right] \qquad (A\text{-}8)$$

$$I_T = 6\left(\frac{D}{T}\right)^2\left[1 - 2\frac{D}{T} + \left(1 + 2\frac{D}{T}\right)e^{-T/D}\right] \qquad (A\text{-}9)$$

$$I_Q = 12\left(\frac{D}{T}\right)^2\left\{2\frac{D}{T} - 6\left(\frac{D}{T}\right)^2 + \left[1 + 4\frac{D}{T} + 6\left(\frac{D}{T}\right)^2\right]e^{-T/D}\right\} \qquad (A\text{-}10)$$

The results were initially applied to predict the false alarm probability. For the case in which the noise power envelope had a low coefficient of variation, the normal density was employed for the basis function, and the false alarm probability is then given by

$$P_F = Q(\gamma) + \left[\frac{\alpha_3}{6}\left(\gamma^2 - 1\right) + \frac{\alpha_4 - 3}{24}\,\gamma\left(\gamma^2 - 3\right)\right] Z(\gamma) \qquad (A\text{-}11)$$

where α_3 is the skewness coefficient of the analog output, i.e. $\mu_{3Z} \div \sigma_Z^3$

α_4 is the kurtosis of the output, i.e., $\mu_{4Z} \div \sigma_Z^4$

Table A-1 shows results for a case in which the noise power envelope is a chi-square process with 100 degrees of freedom. The table also shows P_F for a Gaussian input in the second column.

Table A-1. False Alarm Probability

	False alarm probability						
	Gauss.	Chi-squared envelope, d.f. = 100					
Y	---	D/T→∞	D/T = 1	D/T = .3	D/T = .1	D/T = .03	D/T = 0
0.5	.3085	.3085	.3089	.3095	.3100	.3102	.3103
1.0	.1587	.1585	.1592	.1600	.1606	.1609	.1611
1.5	.06681	.06681	.06730	.0679	.0684	.0686	.0687
2.0	.02275	.02291	.02312	.0234	.0236	.0238	.0238
2.5	.006210	.00633	.00640	.00649	.00658	.00663	.00665
3.0	.001350	.001355	.00139	.00143	.00146	.00148	.00149

For the case D/T→∞, the power envelope is a random variable rather than a random process, and it can be shown that P_F is independent of the envelope distribution, and that it is equal to that for a Gaussian input. The Table shows good agreement between the values in the Gauss and D/T→∞ columns. Since the difference in output moments of second or higher order are the most pronounced for these two cases, it is concluded that the figures in the other columns are also accurate.

For values of γ greater than 3.5, however, the predicted value of P_F for $D/T \to \infty$ diverge appreciably from the Gauss input values. This can be anticipated from the small number of terms in the expansion and the distance from the center of the distribution. The remaining columns show that P_F increases inversely with the D/T ratio.

The right-most column of Table A-1 shows P_F for the case of very fast power envelope fluctuations. These results were calculated from (5.19).

The case of the low-fluctuation envelope is important from the theoretical point of view, but of limited interest from the operational point of view because of the very small changes of probability values.

For more general application, the basis density employed is that for the output (denoted by PW) of the analog when the power envelope is a random variable. For this case, the expression for the false alarm probability is

$$P_F = \sum_{i=1}^{4} a_i \, m_{iP} \, I_i \qquad \text{(A-12)}$$

where a_i is the i^{th} weighting coefficient found by solving (3.6) of Ref. 1.

m_{iP} is the i^{th} moment of the envelope variate

$f_w()$ is the normal density function with mean $m_w = -\beta\sqrt{1+n^{-1}}$, and variance $\frac{1+m^{-1}}{WT}$

$$I_i = m_w^{-i} \sum_{j=0}^{i} C_j^i \, (-\gamma)^j L_j$$

AD-A092 711 BOLT BERANEK AND NEWMAN INC ARLINGTON VA F/G 9/5
EFFECTS OF INPUT POWER FLUCTUATION ON PASSIVE SONAR RECEIVER PE--ETC(U)
SEP 80 M MOLL, D D GOODMAN N00014-79-C-0446
UNCLASSIFIED BBN-4262 NL

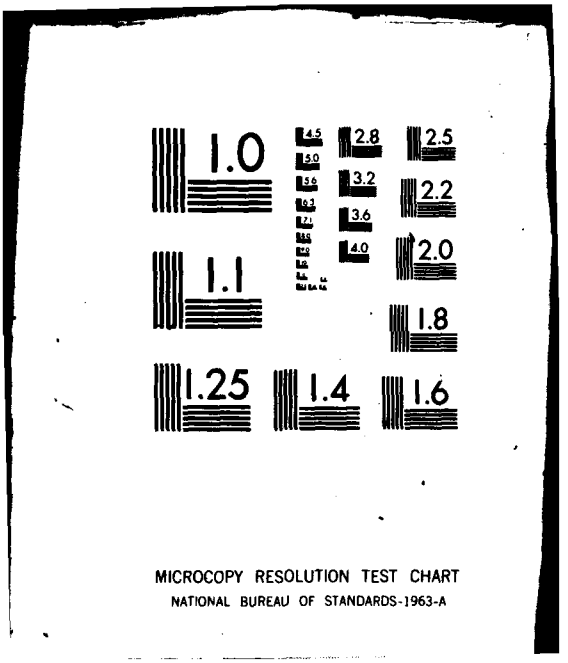
1.0
1.1
1.25
1.4
1.6
1.8
2.0
2.2
2.5
2.8
3.2
3.6
4.0
4.5
5.0
5.6
6.3
7.1
MICROCOPY RESOLUTION TEST CHART
NATIONAL BUREAU OF STANDARDS-1963-A

A recursion formula was derived for L_j:

$$L_j = \gamma^{j-1} Z(\gamma) + (j-1)L_{j-2} \qquad \text{(A-13)}$$

where $Z(\gamma)$ is the normal density function for zero mean, unit variance

$$L_o = Q(\gamma) \qquad \text{(A-14)}$$

The results were applied to a case in which the power envelope process is chi-squared with 100 degrees of freedom, and $\gamma = 1$. The results are shown in Table A-2, which also shows results using the normal basis for the same case.

Table A-2

P_F calculations for n=100, γ=1

False alarm probability

	Gauss	chi-squared envelope, d.f. = 100					
Basis	----	D/T	D/T=1	D/T=1/3	D/T=.3	D/T=.1	D/T=0
PW	.1563	.15865	.1587	.1591	----	.1588	(.1611)
Gauss	.15865	.1585	.1592	----	.1600	.1606	(.1611)

Examination of Table A-2 shows that the gaussian basis yields more accurate results than the PW basis.

The PW basis was also applied to cases of high variability and was found to be unsuitable. Therefore, consideration was given to the use of a simulation or Monte Carlo approach based on the multichannel analog and the compound random process. This approach is covered in the text of this report.

APPENDIX B

Multi-Channel Simulation Software

The software for the multi-channel simulator is composed of seven Fortran programs. These programs can be separated into two groups: random number generators and processor models. The random number generators generate the random processes used as input for the processors. The processes series are written to disk as an intermediate step so that they may be used more than once by the processor programs.

B-1. Random Number Generator Programs

There are three random number generator programs, corresponding to Gaussian, exponential and Chi-squared random variables. Each of the programs receives generation instructions from input at logical I/O unit 5. Each program writes out one file of random variables for every two lines of input from unit 5. The first line assigns values to variables in the Fortran namelist called FACT (see a Fortran manual for an explanation of the namelist I/O feature). This line must begin with a blank immediately followed by "$fact." The line must end with a "$" with the input variable assignments falling in between. (Actually, the namelist input may extend over an arbitrary number of lines, but must begin and end as described.) After namelist input, the program reads the name it will assign to the file it is about to generate. The format for this name is A7 (left-justified) and it may contain any series of seven or less alphanumeric characters, including spaces. After reading this name, the program generates the random variables and writes them out to a disk file. At this point the

program writes out the file name and a summary of namelist variables on unit 6 and then looks to unit 5 for more namelist input. Files are generated in this manner until an end-of-file is detected on unit 5, at which point execution terminates.

NRMGEN — Gaussian Random Number Generator

This program calls the IMSL subroutine GGNPM to generate independent, zero-mean, unit-variance, Gaussian random variables. The loader must be instructed to search the IMSL library for external references when NRMGEN is loaded.

The random variables are written out to a disk file in 1000-variable segments. The operator can instruct the program to square each variable before writing it to disk. The first file is written on logical I/O unit 20. Succeeding files are written on unit 21, unit 22, and so on. Output summarizing the content of each file is written to unit 6.

The following variables comprise the namelist for NRMGEN:

DSEED — a real number between 0 and 2^{31} exclusive that is used to "seed" the generation process. This number should only be specified in the first of the series of namelist input for any particular execution. Otherwise, the random variables may not be independent from file to file. This is because each call to GGNPM uses the seed returned from the last call and

generates a new seed to be used by the succeeding call. Continuity of this chain insures independence. After generation of each file, the last value of DSEED is printed out in the file summary at unit 6. On future executions of NRMGEN, DSEED should be set equal to the last output value of the previous execution to insure that the new files are independent of the previously generated ones. The subroutine GGNPM should not repeat until after 2^{31} variables.

NUM – an integer that specifies the number of 1000-variate segments to be written to the disk file.

SQ – a logical variable that determines whether the variables are squared before being written to disk. This variable should be set equal to ".true." if the variables are to be squared. Otherwise it should be left out of the namelist.

EXPGEN – Exponential Random Number Generator

This progarm calls the IMSL subroutine GGUBS to generate independent random variables uniformaly distributed between 0 and 1. These variables are converted to independent, unit mean exponential variables through the transformation E = EXP(u). the loader must be instructed to search the IMSL library for external references when EXPGEN is loaded.

The random variables are written out to a disk file in 1000-variable segments. The first file is written on logical I/O unit 20. Succeeding files are written on unit 21, unit 22, and so on.

The following variables comprise the namelist input for EXPGEN:

DSEED – a real number between 0 and 2^{31} that is used to "seed" the generation process. Experience has shown that this number should be greater than one billion, to insure independence across files, this number should only be specified in the first of the series of namelist input for any particular execution of EXPGEN (see the instructions for DSEED in NRMGEN).

NUM – an integer that specifies the number of 1000-variate segments to be written to the disk file.

CHIGEN – Chi-Squared Random Number Generator

This program reads previously-generated, independent Gaussian variables as input and generates Chi-squared random variables as output. The block diagram for the generation process is shown in Figure 2.4. The Gaussian variables are input from a file attached to logical I/O unit 30. This file is rewound and read in again from the beginning for every succeeding file of Chi-squareds that is generated. The Chi-squareds are written out to a disk file in 1000-variable segments. The operator has the option of writing the square root of every variable out to disk rather than the variable itself. The first file of Chi-squareds

is written out to logical I/O unit 20. Succeeding files are written out to unit 21, unit 22, and so on.

The following variables comprise the namelist input for CHIGEN:

NDF – the number of degrees of freedom of the Chi-squared series.

NRA – the length of the running average in the generation process.

NUM – the number of 1000-variable segments to be generated

SQ – a logical variable that determines whether the square root of each Chi-squared or the Chi-squared itself is written to disk. This variable should be set to ".true." if square roots are desired. Otherwise, SQ should be left out of the namelist input.

B-2. Multi-Channel Processor Programs

These models simulate the passive sonar detection process. Each model contains 3 channels. Signals representing noise are always input at all three channels. The middle channel may also contain a genuine signal. The channel inputs are processed to detect signals present at the center channel. The outside channels are needed because the detection procedure works by comparing the center channel to the outside ones.

In the interest of computational efficiency, the simulations were divided into four categories and a specialized model was built for each category. The simulations were divided according to whether they were used to estimate detection or false alarm probabilities, and whether the power envelopes of the noise series were fully or only partially correlated across each channel.

Each program is written in Fortran. The programs receive the simulation instructions and parameters (length of simulation, degrees of freedom of the noise envelope, etc.) through the namelist FACT at logical I/O unit 5. Each program reads from unit 5 until the namelist is satisfied (see a Fortran manual for details on how to satisfy a namelist) at which point simulation is begun. After the first simulation the program reads again from unit 5, and performs another simulation. The program ends when an end of file is encountered at unit 5.

MCHCFA — Common Noise Power Envelope False Alarm Model

This model is designed to estimate the false alarm probability of the multichannel processor when the power envelope of the noise is common to all three channels. The block diagram for this model is shown in Figure 5.1. To save CPU time, the squared, zero-mean, unit-variance, Gaussian noise series at the two outside channels are replaced by a series of independent unit-mean, exponential variables before multiplication by the power envelope. The power envelope is always a Chi-squared series generated by the CHIGEN. The input to the center channel is always a series of independent, squared, Gaussian variates.

The following variables comprise the namelist input for MCHCFA:

NCHIF – the logical unit number of the file that contains the power envelope. The default for this variable is 20.

NDF – the number of degrees of freedom in the Chi-squared random variables in the power envelope.

NPRA – the length of the running average in the power envelope.

NRECRA – the length of the rectifier running average in the MC processor.

NSIM – the number (in thousands) of independent observations of the rectifier output.

NC – the number of different values for parameter C in this simulation.

C – this is a vector (maximum length 10) of values for the threshold parameter that is used internally by the processor. False alarm estimates are generated for each value of C during any simulation.

The Gaussian input for MCHDFA is read at unit 30. The exponential input is read at unit 31.

OUTPUT

The probability of false alarms for each value of C constitutes the most important part of the output. This probability is merely the number of detections divided by the number of independent observations. The names of the files used as input, and a summary of the "facts" namelist are also output.

MCHCDT – Common Noise Power Envelope Detection Model

This model is designed to estimate the detection probability of the processor when the power envelope of the noise is common to all channels. The block diagram for this model is shown in figure 6.1. This model is exactly the same as the previous one except that an additional series is added to the center channel to simulate a signal. This additional signal is multiplied by a power envelope that is independent of the noise power envelope. The signal power envelope is generated by the Chi-squared program and is the square root of a Chi-squared series. The two series at the bottom left of Figure 6.1 represent this additional input.

A list of the variables that comprise the namelist follows:

NCHIS – The logical unit number of the file that contains the power envelope of the signal. The default is 40.

NCHIN – the logical unit number of the file that contains the power envelope of the noise. The default of this variable is 20.

NDFS – the number of degrees of freedom in the running average of the signal envelope.

NDFN – the running average in the noise envelope.

NPRAS – the running average in the signal envelope

NRECRA – the length of the running average in the rectifier.

NSIM – the number (in thousands) of independent observations of the rectifier output.

NK – the number of different values for the S/N ration in this simulation.

SN – a vector (maximum length 10) of signal-to-noise ratios. A detection probability is given for each value of S/N.

C – the threshold parameter...used internally by the processor.

OUTPUT

The detection probability for each value of S/N is output along with the names of the files used as input and a summary of the "facts" namelist.

MCHPDT — Partially-Correlated Noise Power Envelope Detection Model

This model is designed to estimate the detection probability of the processor when the power envelopes of the noise inputs are partially correlated across the 3 channels. The block diagram for this model is shown in Figure 7.2. Note that the outside channels cannot be combined for this model because of their different power envelopes.

The generation procedure is internal to MCHDDT and not a part of CHIGEN. Only one series of independent, zero-mean, unit-variance, Gaussian variates is required as input by this procedure. As with MCHCDT, the power envelope for the signal is Chi-squared and independent of the noise power envelope.

A list of the variables that comprise the namelist input follows:

NCHIS — the logical I/O unit number of the file that contains the signal power envelope series.

NCHIN — the logical I/O unit number of the file that contains the series of independent Gaussian variates that drive the partially correlated Chi-squared generator.

NDFS — the number of degrees of freedom of the power envelope of the signal.

NDFN — the number of degrees of freedom of the power envelope of the noise.

NPRAS – the length of the running average in the power envelope of the signal.

NPRAN – the length of the running average in the power envelope of the noise.

NRECRA – the length of the running average following the rectifier.

NSIM – the number (in thousands) of independent observations of rectifier output. The time steps between observations to achieve independence is computed internally by the program is NRECRA + ma_X (NPRAS, NPRAN).

NK – the number of different values for SN in this simulation.

SN – a vector S/N values (maximum length 10).

C – the threshold parameter used internally by the processor.

OUTPUT

The detection probability for each value of SN is output along with the names of files used as input and a summary of the "facts" namelist.

MCHPFA – Partially Correlated Noise Power Envelope False Alarm Model

This model is designed to estimate the false alarm probability of the processor when the power envelope of the noise is partially correlated across the 3 channels. The only difference between this model and MCHPDT is that there is no signal series input to the center channel in this model. No additional block diagram is shown for this model.

A list of the input variables in the namelist for this program follows:

NCHIN – The logical I/O unit of the file that contains the series of independent Gaussians that drive the partially correlated Chi-squared generator.

NDFN – the number of degrees of freedom of the power envelope of the signal.

NPRAN – the length of the running average in the power envelope of the noise.

NRECRA – the length of the running average following rectification.

NK – the number of different values for the parameter C.

C – a vector of values for the threshold parameter (maximum length 10).

OUTPUT

The false alarm probability for each value of C is output along with the names of the files used as input and a summary of the variables in the "facts" namelist.

Distribution List
for
"Effects of Input Power Fluctuations on Passive Sonar Receiver Performance"

All addressees receive one copy unless otherwise specified

Dr. Thomas O. Mottl
The Analytic Sciences Corporation
Six Jacob Way
Reading, MA 01867

Naval Ocean Systems Center
Code 6212
San Diego, CA 92152

Naval Surface Weapons Center
White Oak Laboratory
Code U-20
Silver Spring, MD 20910 2 copies

Dr. Yaakov Bar-Shalom
The University of Connecticut
Department of Electrical Engineering
and Computer Science
Box U-157
Storrs, CT 06268

Mr. J. Conrad
Naval Intelligence Support Center
Code 20
Suitland, MD 20390

Dr. V. T. Gabriel
General Electric Company
Sonar Systems Engineering
Farrell Road Plant
Building 1, Room D6
Syracuse, NY 13201

Naval Air Development Center
Warminster, PA 18974

Naval Electronics Systems Command
Washington, DC 20360
Code 320
PME-124

Naval Research Laboratory
Washington, DC 20375
Code 2627, Code 5308, Code 7932

Naval Sea Systems Command
Washington, D.C. 20360
Code 63R-1, Code 63R-16

Defense Technical Information Center
Cameron Station
Alexandria, VA 22314 12 copies

Center for Naval Analyses
2000 North Beauregard Street
Alexandria, VA 22311

Office of Naval Research
Code 431
Arlington, VA 22217 2 copies

Dr. Byron D. Tapley
The University of Texas at Austin
Department of Aerospace Engineering
and Engineering Mechanics
Austin, TX 78712

Dr. Fred W. Weidmann
Tracor, Inc.
Tracor Sciences & Systems
6500 Tracor Lane
Austin, TX 78721

Dr. C. Carter
Naval Underwater Systems Center
New London Laboratory
Code 313
New London, CT 06320

Naval Underwater Systems Center
Code 352
Newport, RI 02840

Dr. J. Anton
Systems Control, Inc.
1801 Page Mill Road
Palo Alto, CA 94304

Office of Naval Research Eastern
Building 14, Section D
Regional Office
666 Summer Street
Boston, MA 02210

Dr. R. Cavanagh
Planning Systems, Inc.
Suite 600 7900 West Park Drive
McLean, VA 22102

Distribution List (Cont'd)

Naval Postgraduate School
Monterey, CA 93940
Technical Library
Dr. H. Titus
Dr. N. Forrest
Dr. G. Sackman

Applied Physics Laboratory
Johns Hopkins University
Johns Hopkins Road
Laurel, MD 20810

Summit Research Corporation
1 West Deer Park Avenue
Gaithersburg, MD 20760

Massachusetts Institute of Technology
Department of Ocean Engineering
Cambridge, MA 02139
Dr. Psaraftis